ISTANBUL TECHNICAL UNIVERSITY ★ GRADUATE SCHOOL

A ROADMAP FOR BREAST CANCER MICROWAVE HYPERTHERMIA TREATMENT PLANNING AND EXPERIMENTAL SYSTEMS

M.Sc. THESIS

Meltem Duygu ŞAFAK

Department of Electronics and Communication Engineering

Telecommunications Engineering Programme

JULY 2024

ISTANBUL TECHNICAL UNIVERSITY ★ GRADUATE SCHOOL

A ROADMAP FOR BREAST CANCER MICROWAVE HYPERTHERMIA TREATMENT PLANNING AND EXPERIMENTAL SYSTEMS

M.Sc. THESIS

Meltem Duygu ŞAFAK
(504191326)

Department of Electronics and Communication Engineering

Telecommunications Engineering Programme

Thesis Advisor: Assist. Prof. Dr. Gülşah YILDIZ ALTINTAŞ

JULY 2024

İSTANBUL TEKNİK ÜNİVERSİTESİ ★ LİSANSÜSTÜ EĞİTİM ENSTİTÜSÜ

MEME KANSERİ MİKRODALGA HİPERTERMİSİNDE TEDAVİ PLANLAMA VE DENEYSEL SİSTEMLER İÇİN BİR YOL HARİTASI

YÜKSEK LİSANS TEZİ

Meltem Duygu ŞAFAK
(504191326)

Elektronik ve Haberleşme Mühendisliği Anabilim Dalı

Telekomünikasyon Mühendisliği Programı

Tez Danışmanı: Assist. Prof. Dr. Gülşah YILDIZ ALTINTAŞ

TEMMUZ 2024

Meltem Duygu ŞAFAK, a M.Sc. student of ITU Graduate School student ID 504191326 successfully defended the thesis entitled "A ROADMAP FOR BREAST CANCER MICROWAVE HYPERTHERMIA TREATMENT PLANNING AND EXPERIMENTAL SYSTEMS", which he/she prepared after fulfilling the requirements specified in the associated legislations, before the jury whose signatures are below.

Thesis Advisor :	**Assist. Prof. Dr. Gülşah YILDIZ ALTINTAŞ** Istanbul Technical University	.....
Jury Members :	**Assist. Prof. Dr. Cemanur AYDINALP** Istanbul Technical University	.....
	Prof. Dr. Hülya ŞAHİNTÜRK Yıldız Technical University	.....

Date of Submission : **24 May 2024**
Date of Defense : **4 July 2024**

To my parents and advisor,

FOREWORD

I am grateful to my supervisor, Assist. Prof. Dr. Gülşah YILDIZ ALTINTAŞ, for accepting me as a M.Sc. student in Telecommunications Engineering at Department of Electronics and Communication in Istanbul Technical University. I always admired her determination, her ability to overcome difficulties and goal oriented work. I appreciate her for her guidance in every aspect of my M.Sc. and supporting my personal and academic life. She inspired me with her hard-working nature. I will always appreciate all the advice and guidance and cherish our time together.

I would like to thank my fellow graduate students, for the valuable discussions and conversations we have made on our studies as well as on life itself. I consider myself fortunate to have you by my side through the difficulties of the academic life.

Special thanks to Assoc. Prof. Dr. Tuba YILMAZ ABDOLSAHEB and Assist. Prof. Dr. Cemanur AYDINALP for the valuable guidance through my M.Sc. studies.

Last but most importantly, I am indebted to my parents, Ayfer ŞAFAK and Hüseyin ŞAFAK for raising me and supporting me at all times. Also I would like to thank my sister Gül Ezgi EZERCAN who supported me through my studies and hardships. I will always be grateful to my family for their support during my studies and I will treasure their love in life. I couldn't have overcome the difficulties I have faced without their love and support. I am very lucky to call them my family and to have them in my life. I hope to live a life that makes them proud.

July 2024

Meltem Duygu ŞAFAK
(Electrical & Electronics Engineer)

TABLE OF CONTENTS

ABBREVIATIONS

SAR	**:** Specific Absorption Rate
avSAR	**:** Average Specific Absorption Rate
HP	**:** Heating Potential
TBR_S	**:** Target-to-Breast SAR Ratio
TBR_T	**:** Target-to-Breast Temperature Ratio
HTQ_S	**:** Hotspot-to-Target SAR Ratio
HTQ_T	**:** Hotspot-to-Target Temperature Ratio
HTP	**:** Hyperthermia Treatment Planning
MH	**:** Microwave Hyperthermia
PSO	**:** Particle Swarm Optimization
CNN	**:** Convolutional Neural Network
EM	**:** Electromagnetic
TR	**:** Time reversal
iw-PSO	**:** Inertia-weighted particle swarm optimization
HTP	**:** Hyperthermia treatment planning
FD	**:** Finite difference
FEM	**:** Finite element methood
ISM	**:** Industrial, Scientific, and Medical
MRI	**:** Magnetic resonance imaging
TBR	**:** Target-to-breast ratio
HTQ	**:** Hotspot-to-target quotient
CA	**:** Circular applicator
LA	**:** Linear applicator
TC	**:** Tumor coverage
FOCO	**:** Optimal Constrained Power Focusing
CP	**:** Convex Programming
NP-hard	**:** Non-Deterministic Polynomial-time Hard
DE	**:** Differential Evolution
RF	**:** Radio Frequency
ReLu	**:** Rectified Linear Unit
CP	**:** Convex Programming

SYMBOLS

2D	: Two dimensional
3D	: Three dimensional
α_i	: Amplitude of $i^t h$ antenna
ϕ_i	: Phase of $i^t h$ antenna
ϕ_v	: Vertical phase difference
ϕ_h	: Horizontal phase difference
θ	: Applicator rotation angle
$\mathbf{E_{tot}}$	: The total electric field
$\mathbf{E_x}$, $\mathbf{E_y}$, $\mathbf{E_z}$	: Electric field components
C_p	: The specific heat capacity
ρ	: The density
K	: The thermal conductivity
T	: The temperature
T_b	: The blood temperature
A_0	: The metabolic heat generation
Q_m	: The metabolic heat generation
Q_0	: The heating potential
B	: The capillary blood perfusion coefficient
ε_∞	: The high-frequency permittivity
$\Delta\varepsilon$	: The difference between the high frequency and the static perittivity
σ_s	: The static conductivity
τ	: The relaxation time
ε_r	: The Relative permittivity
σ	: The conductivity
$\mathbf{w}$	: Inertia weight
$\mathbf{w_{damp}}$	: Damping constant
$\mathbf{S_{ii}}$	: S-parameters

LIST OF TABLES

Page

LIST OF FIGURES

Page

A ROADMAP FOR BREAST CANCER MICROWAVE HYPERTHERMIA TREATMENT PLANNING AND EXPERIMENTAL SYSTEMS

SUMMARY

Breast cancer affects approximately 2.5 million women each year and can be fatal if not treated correctly. However, with proper treatment, survival rates are very high. Common treatments include invasive surgical procedures such as lumpectomy or mastectomy, and non-surgical methods like radiotherapy, chemotherapy, and other anti-cancer agents. Enhancing the efficiency of these treatments can mitigate the economic and psychological impacts on patients. Studies have shown that artificial hyperthermia, which involves elevating the temperature in cancerous regions, can enhance the effectiveness of these modalities. Microwave breast hyperthermia (MH) aims to raise the temperature at the tumor site above normal levels. During this procedure, unwanted hotspots can occur, and the main goal of MH is to avoid these while achieving the necessary temperature at the tumor. The specific absorption rate (SAR), which measures the absorbed heat energy per kilogram of breast tissue, needs to be carefully controlled. The design of the MH applicator is crucial for focusing energy on the target effectively. Despite variations in hyperthermia treatment planning (HTP) for each patient, the MH applicator must be effective across different breast models and tumor types.

The optimization and predictive modeling of temperature-dependent dielectric properties in microwave hyperthermia treatments, focusing primarily on breast cancer is investigated. This research aims to enhance the efficacy and precision of hyperthermia therapy through a combination of computational simulations, empirical data analysis, and deep learning techniques. This study is a comprehensive exploration of microwave hyperthermia treatment planning for breast cancer, focusing particularly on the critical consideration of temperature-dependent dielectric properties (TD-DP) within this context. In addition, an experimental study was conducted to realize computational analysis. It delves into multifaceted aspects of microwave hyperthermia treatment, spanning from the optimization of antenna parameters to the prediction of electromagnetic distribution through innovative methodologies like the U-Net architecture.

One of the central inquiries is the optimization of antenna parameters concerning temperature-dependent dielectric properties. This study delves into the intricacies of how variations in these properties can influence treatment outcomes and efficacy. By analyzing these relationships, this thesis aims to establish optimized antenna configurations that maximize treatment precision and effectiveness.

Deep learning, particularly convolutional neural networks (CNN), emerges as a powerful tool within this framework. By leveraging CNNs, this thesis investigates

methods to use as a preliminary step of hyperthermia antenna excitation parameter selection. This integration of cutting-edge artificial intelligence techniques holds promise for streamlining and automating aspects of treatment planning, thereby potentially reducing human error and enhancing overall efficiency. Particularly, the U-Net model's potential is studied in automating the generation of electric field distribution of a particular dielectric distribution such as the breast tissue. By harnessing the capabilities of artificial intelligence, particularly in image analysis and processing, it aims to develop more robust and efficient methodologies for treatment planning. The integration of the U-Net model represents a significant advancement in this regard, promising to streamline processes and enhance treatment precision.

To verify the performed computational simulations, an experimental microwave hyperthermia system was built. A circular array of 12 dipole antennas was installed in this system to experiment on tissue-mimicking phantom to gather information on microwave hyperthermia treatment system. Therefore, a significant amount of information on microwave hyperthermia is gathered through this experiment.

Ultimately, the overarching objective of the thesis is to advance microwave hyperthermia treatment planning for breast cancer by improving both precision and efficacy. By synthesizing insights from diverse disciplines such as electromagnetics and deep learning, this thesis seeks to push the boundaries of current practices and pave the way for more effective treatment strategies. Through its meticulous analysis and innovative approaches, the thesis contributes valuable knowledge and methodologies to the ongoing quest for improved cancer therapies.

To achieve that, COMSOL Multiphysics software is utilized to simulate the electromagnetic and thermal behavior of breast tissue during hyperthermia treatment. These simulations consider both constant and temperature-dependent dielectric properties. Empirical data is collected using phantoms that mimic the dielectric properties of breast tissue. Temperature distributions are recorded and compared with simulated results to validate the models. U-Net architecture, an encoder-decoder model, is used to predict electromagnetic field distributions, significantly reducing the computational workload and enhancing the accuracy of treatment planning.

This research underscores the importance of optimizing antenna configurations to achieve targeted heating while minimizing damage to surrounding healthy tissues. Variations in tissue properties with temperature are crucial for effective hyperthermia treatment, and modeling these changes can lead to better treatment protocols. Despite the promising results, the transition of high-precision hyperthermia into clinical practice faces challenges such as technical complexities, high computational costs, and the need for further validation and optimization.

Future research should focus on overcoming the remaining technical and computational barriers, refining the proposed methods, and conducting extensive validation studies to facilitate the clinical adoption of high-precision hyperthermia treatments.

This thesis represents a significant step towards improving the precision and effectiveness of hyperthermia therapy, offering a comprehensive framework for future advancements in this field.

MEME KANSERİ MİKRODALGA HİPERTERMİSİNDE TEDAVİ PLANLAMA VE DENEYSEL SİSTEMLER İÇİN BİR YOL HARİTASI

ÖZET

Bu çalışmada, meme kanseri tedavisinde kullanılan mikrodalga hipertermi (MH) uygulamalarında sıcaklığa bağlı dielektrik özelliklerin optimizasyonu ve öngörücü modellemesini kapsamlı bir şekilde ele almaktadır. Araştırmanın amacı, hesaplamalı simülasyonlar, ampirik veri analizi ve derin öğrenme teknikleri kullanılarak hipertermi tedavisinin etkinliğini ve hassasiyetini artırmaktır.

Meme kanseri her yıl yaklaşık 2,5 milyon kadını etkilemekte ve doğru tedavi edilmediğinde ölümcül olabilmektedir. Ancak, uygun tedavi yöntemleri ile hayatta kalma oranları oldukça yüksektir. Yaygın tedavi yöntemleri arasında lumpektomi veya mastektomi gibi invaziv cerrahi işlemler ve radyoterapi, kemoterapi ve diğer anti-kanser ajanları gibi cerrahi olmayan teknikler bulunmaktadır. Tedavilerin verimliliğini artırmak, hastaların karşı karşıya kaldığı ekonomik ve psikolojik yükleri hafifletebilir. Yapılan çalışmalar, kanserli bölgelerde sıcaklık artırılarak uygulanan yapay hiperterminin bu tedavi yöntemlerinin etkinliğini artırabileceğini göstermiştir.

Mikrodalga meme hipertermisi (MH), tümör bölgesinde sıcaklığı normal seviyelerin üzerine çıkarmayı hedefler. Bu işlem sırasında istenmeyen sıcak noktalar oluşabilir ve MH'nin ana amacı, tümörde gerekli sıcaklığı elde ederken bu sıcak noktaları önlemektir. Meme dokusunun kilogram başına emilen ısı enerjisini ölçen spesifik absorpsiyon oranı (SAR) dikkatle kontrol edilmelidir. MH uygulayıcısının tasarımı, enerjinin hedefe etkili bir şekilde odaklanması için çok önemlidir. Her hasta için hipertermi tedavi planlamasında (HTP) değişiklikler olmasına rağmen, MH uygulayıcısı farklı meme modelleri ve tümör tipleri için etkili olmalıdır.

Mikrodalga hipertermi tedavilerinde sıcaklık bağımlı dielektrik özelliklerin optimizasyonu ve öngörücü modellemesi, özellikle meme kanseri odaklı olarak incelenmektedir. Bu araştırma, hesaplamalı simülasyonlar, deneysel veri analizi ve derin öğrenme tekniklerinin bir kombinasyonu aracılığıyla hipertermi tedavisinin etkinliğini ve hassasiyetini artırmayı amaçlamaktadır. Bu çalışma, bu bağlamda sıcaklık bağımlı dielektrik özelliklerinin kritik bir şekilde ele alındığı meme kanseri için mikrodalga hipertermi tedavi planlamasının kapsamlı bir keşfidir. Ayrıca, hesaplamalı analizin gerçekleştirilmesi için deneysel bir çalışma yapılmıştır. Mikrodalga hipertermi tedavisinin birçok yönünü, anten parametrelerinin optimizasyonundan U-Net mimarisi gibi yenilikçi metodolojilerle elektromanyetik dağılımın tahminine kadar kapsamaktadır.

Anten parametrelerinin sıcaklık bağımlı dielektrik özelliklerine göre optimizasyonu, merkezi soruşturmalardan biridir. Bu çalışma, bu özelliklerdeki değişimlerin tedavi sonuçları ve etkinliği üzerinde nasıl etkili olabileceğinin incelenmesine odaklanır. Bu

ilişkileri analiz ederek, bu tez, tedavi hassasiyetini ve etkinliğini maksimize eden optimize anten yapılandırmalarını belirlemeyi amaçlamaktadır.

Ayrıca, bu çalışma, özellikle meme mikrodalga hipertermi uygulamaları için özel olarak tasarlanmış doğrusal anten dizilerinin kullanımını araştırmaktadır. Bu, sadece bu dizilerin fiziksel özelliklerini anlamakla kalmaz, aynı zamanda bunları tedavi planlama süreçlerine sorunsuz bir şekilde entegre etmeyi ve tedavi sonuçlarını artırmak için kullanır. Ayrıntılı bir incelemeyle, bu tür anten yapılandırmalarının meme kanseri tedavisi bağlamında avantajları ve sınırlamaları analiz edilmektedir.

Bu çerçevede özellikle derin öğrenme, özellikle evrişimli sinir ağları (CNN), güçlü bir araç olarak ortaya çıkar. CNN'leri kullanarak, tez hipertermi anten uyarıcı parametre seçimi yöntemlerini araştırır. Bu, tedavi planlamanın bazı yönlerini akıllıca yaparak ve otomatikleştirerek insan hatalarını potansiyel olarak azaltarak ve genel verimliliği artırarak, keskin bir yapay zeka tekniklerinin entegrasyonunu içerir. Özellikle, hipertermi parametrelerinin otomatik oluşturulmasında U-Net modelinin potansiyeli incelenir. Yapay zeka yeteneklerinden, özellikle görüntü analizi ve işleme alanında, faydalanarak, tedavi planlama için daha sağlam ve verimli metodolojiler geliştirmeyi amaçlamaktadır. U-Net modelinin entegrasyonu, bu açıdan önemli bir ilerleme sunarak, süreçleri akıcı hale getirme ve tedavi hassasiyetini artırma vadeder.

Yapılan hesaplamalı simülasyonları doğrulamak için deneysel bir mikrodalga hipertermi sistemi kurulmuştur. Bu sistemde, doku taklit eden fantom üzerinde deney yapmak amacıyla 12 dipol antenli dairesel bir dizi kurulmuştur ve mikrodalga hipertermi tedavi sistemi hakkında bilgi toplamak için kullanılmıştır. Bu nedenle, bu deney yoluyla mikrodalga hipertermi hakkında gelecek çalışmalarda kullanmak üzere önemli miktarda bilgi toplanmıştır.

Bu hedefe ulaşmak için, hipertermi tedavisi sırasında meme dokusunun elektromanyetik ve termal davranışını simüle etmek için COMSOL Multiphysics yazılımı kullanılmaktadır. Bu simülasyonlar, hem sabit hem de sıcaklığa bağlı dielektrik özellikleri dikkate almaktadır. Meme dokusunun dielektrik özelliklerini taklit eden fantomlar kullanılarak ampirik veriler toplanmaktadır. Sıcaklık dağılımları kaydedilip simüle edilen sonuçlarla karşılaştırılarak modeller doğrulanmaktadır. U-Net mimarisi, bir kodlayıcı-çözücü model olarak elektromanyetik alan dağılımlarını tahmin etmek için kullanılır, bu da hesaplama iş yükünü önemli ölçüde azaltır ve tedavi planlamasının doğruluğunu artırır.

Araştırmanın önemli bir bulgusu, çevredeki sağlıklı dokulara zarar vermeden hedeflenen ısıtmayı sağlamak için anten konfigürasyonlarının optimize edilmesinin kritik olduğudur. Sıcaklığa bağlı doku özelliklerindeki değişiklikler, etkili hipertermi tedavisi için çok önemlidir ve bu değişikliklerin modellenmesi daha iyi tedavi protokollerine yol açabilir. Hastaya özel tedavi planlamasında kullanılan modellerin hassasiyetinin artırılması, tedavi sonuçlarının iyileştirilmesi açısından büyük önem taşımaktadır.

Bununla birlikte, yüksek hassasiyetli hiperterminin klinik uygulamaya geçişi, teknik karmaşıklıklar, yüksek hesaplama maliyetleri ve daha fazla doğrulama ve optimizasyon gereksinimi gibi zorluklarla karşı karşıyadır. Klinik uygulamalara entegrasyonun başarısı, bu teknik ve hesaplama engellerinin aşılmasına bağlıdır.

Gelecekteki araştırmalar, bu engellerin üstesinden gelmek, önerilen yöntemleri rafine etmek ve yüksek hassasiyetli hipertermi tedavilerinin klinik olarak benimsenmesini kolaylaştırmak için kapsamlı doğrulama çalışmalarını yürütmek üzerine odaklanmalıdır. Özellikle, hasta modellerinin daha geniş bir yelpazede test edilmesi ve farklı tümör tipleri üzerinde uygulamaların optimize edilmesi gerekmektedir.

Sonuç olarak, bu tez, hipertermi terapisinin hassasiyetini ve etkinliğini artırma yolunda önemli bir adımı temsil etmekte ve bu alandaki gelecekteki ilerlemeler için kapsamlı bir çerçeve sunmaktadır. Geliştirilen yöntemlerin ve elde edilen bulguların klinik uygulamalara entegrasyonu, meme kanseri tedavisinde yeni ufuklar açabilir ve hastaların yaşam kalitesini önemli ölçüde artırabilir. Bu çalışma, hipertermi tedavilerinde kişiye özel yaklaşımlar geliştirilmesine yönelik önemli bir katkı sunmaktadır ve bu alandaki gelecekteki araştırmalar için sağlam bir temel oluşturmaktadır. Gelecek araştırmalarda, önerilen yöntemlerin daha da geliştirilmesi, teknik ve hesaplama engellerinin aşılması ve klinik doğrulama çalışmalarının genişletilmesi gerekmektedir.

1. INTRODUCTION

The utilization of Microwave Hyperthermia (MH) treatment represents a promising strategy intended to raise the temperature of malignant tumors, thereby inducing cellular destruction. Whether applied independently or in conjunction with modalities such as chemotherapy, MH seeks to selectively elevate the temperature of target tissues. The significance of this approach lies in its capacity to enhance the sensitivity of cancer cells to radiation, thereby rendering them more susceptible to eradication.

In the implementation of MH, an external microwave heat source is introduced via antenna excitation surrounding the designated tissue, thereby influencing temperature stability. The Specific Absorption Rate (SAR), which quantifies this heat deposition, necessitates meticulous optimization to precisely focus energy within the tumor site. However, achieving such precision poses a challenge, contingent upon factors such as tissue composition and applicator design, particularly in maintaining normothermic conditions within healthy tissues.

SAR is contingent upon the distribution of the electric field, which, in turn, is influenced by tissue dielectric properties (DP) induced by the microwave antennas. In the planning of hyperthermia treatment, modeling the DP of breast tissue holds significant importance for optimizing hyperthermia parameters to ensure effective tumor heating. It has been demonstrated that tissue DP undergoes changes with temperature variations occurring during hyperthermia treatment, thus necessitating treatment planning that accounts for these fluctuations. However, in many studies on microwave hyperthermia, the temperature dependency of DP is often overlooked. This study aims to investigate the impact of neglecting temperature-dependent DP (TD-DP) of breast tissues in microwave hyperthermia treatment.

In hyperthermia treatment, the most crucial tissues will be those that are more heterogeneous. Homogeneous tissues will be minimally affected by this condition. An example of heterogeneous tissue is breast tissue. This study especially focuses on

the effect of temperature-dependent dielectric properties in breast cancer hyperthermia treatment.

Breast cancer ranks as the most prevalent form of cancer among women worldwide, constituting nearly 30% of all malignancies [1]. According to World Health Organization data from 2020, approximately 2.3 million women received diagnoses of breast cancer, resulting in 685,000 breast cancer-related fatalities [2]. Breast cancer does not discriminate by age or geographical location, posing a risk to women across all demographics. Timely diagnosis significantly enhances treatment efficacy, with a reported survival rate of 90% for early-stage cases. Invasive treatments such as mastectomy (complete breast removal) or lumpectomy (partial breast removal) are commonly employed. Following tumor removal, radiation therapy is often administered to mitigate further risks. Anti-cancer medications, including hormone therapy, chemotherapy, and targeted biologic therapy, are utilized to prevent cancer spread, administered orally or intravenously. However, the duration of these treatments varies based on therapy effectiveness, with each iteration imposing escalating financial burdens on patients and healthcare systems, alongside significant psychological strain on patients and their families.

The primary objective of hyperthermia studies is to raise tissue temperature between 40°C and 43°C [3,4]. Further elevation of heat to the tumor leads to the denaturation of nucleic, cytoplasmic, or membrane proteins, causing a cytotoxic effect on malignant cells; surpassing a threshold temperature, typically 45°C, is defined as thermal ablation, which can serve as a standalone treatment technique. Given that hyperthermia entails the destruction of targeted cells, precise focusing of microwave energy onto the target region is imperative. A critical aspect of hyperthermia involves elevating the temperature of the targeted area while ensuring that non-targeted/healthy regions remain below denaturation thresholds.

The steps involved in proper hyperthermia treatment planning (HTP) encompass several stages. Following the diagnosis of a malignant tumor, detailed imaging of the affected body part is obtained, and tissues are segmented [5]–[8]. Subsequently, accurate dielectric and thermal properties are assigned to each tissue type [9]–[15].

Antenna excitations are then appropriately applied to achieve controlled tumor temperature elevation while preventing hotspots in healthy tissue, thereby effectively focusing the Specific Absorption Rate (*SAR*) on the target. Consequently, optimization of antenna excitation parameters (phase and power) becomes imperative for efficient energy deposition on the target while minimizing external energy exposure to healthy tissue. It is crucial to customize HTP to meet each patient's unique requirements, as a one-size-fits-all approach is not feasible. Despite numerous studies on hyperthermia, clinically available products remain elusive, necessitating further refinement of hyperthermia and HTP techniques.

In addition to breast cancer treatment, MH finds application in the treatment of various other diseases, including malignant tumors in the brain, bones, neck, and bladder, as well as benign tumors in prostate tissues. For instance, a beamforming method was proposed for non-invasive MH of pediatric brain cancer [16], while the efficacy of combined MH and chemotherapy for bladder cancer treatment was investigated in clinical trials [17]. MH has also been proposed for enhancing muscle recovery after injuries [18].

1.1 Purpose of Thesis

Within the outlined context, the overarching objective of this dissertation is to enhance microwave hyperthermia treatment planning for breast cancer and form a pathway for a successful experimental system. To achieve this goal, three main studies were conducted.

The first part of the thesis emphasizes the importance of temperature-dependent dielectric properties in influencing thermal energy distribution during microwave hyperthermia, crucial for refining treatment strategies and improving patient outcomes. Understanding these properties allows clinicians to better manage tissue response variations, aiding in the development of optimized, patient-specific treatment protocols that maximize therapeutic benefits and minimize risks. The research also highlights the value of sophisticated modeling techniques to simulate the interactions between microwave energy and biological tissues, enabling the exploration of diverse treatment scenarios beyond empirical experimentation. This part aims to elucidate the role of

temperature-dependent dielectric properties and pave the way for innovations in cancer therapy and personalized medicine.

In the second part of this thesis, We investigated using a circular array of antennas for breast microwave hyperthermia. Optimizing antenna excitation for these arrays is complex due to the intricate computation of the electric field within the breast, so we utilized COMSOL Multiphysics for effective E-Field distribution simulation. Employing global particle swarm optimization (PSO) techniques, known for their rapid convergence in multi-parameter optimization, we encountered challenges due to PSO's dependency on initial values, requiring multiple iterations and increasing computational overhead. To address this, we introduced a deep learning-based method using a CNN model trained on dielectric properties from the University of Wisconsin breast cancer repository [19] to predict E-Field distribution, offering a promising alternative for hyperthermia treatment planning.

The third part of the thesis aims to build a system that can be used in preclinical experiments for microwave hyperthermia. By explaining the sub-parts of this experimental system one by one, the purpose is to create a road map for those who want to work on MH. In addition, the stages of preparing tissue-mimicking phantoms, which are indispensable for preclinical experiments, are also explained. In line with these explanations, a phantom mimicking the fat tissue was produced and microwave hyperthermia was applied selectively to the fat phantom in the specified experimental system. The system was verified by comparing the temperature distribution taken with a thermal camera with the previously computed distribution.

1.2 Literature Review

Optimization of microwave hyperthermia (MH) applicator antenna excitation involves two sequential steps: first, selecting the MH applicator design, followed by applying an optimization algorithm for antenna excitation. Therefore, the choice of MH applicator holds significant importance. Circular-shaped applicators (CA) are the prevailing choice in breast MH applications [20]–[22]. The inherent symmetry of CA facilitates comprehensive coverage of breast tissue. Typically, the breast is positioned within a cavity encircled by multiple antennas, and then the amplitude and phase are tailored

to each antenna in a patient-specific manner. Two-dimensional specific absorption rate (SAR) focusing algorithms developed by Iero et al. [20,22] have been extended to three-dimensional scenarios, termed as optimal constrained power focusing (FOCO) [23]. Previous works often utilized simple or semi-realistic phantoms; for instance, Bellizzi et al. [24] employed a multi-frequency 2D FOCO approach, evaluating its effectiveness across different breast densities. Other studies by Elkayal et al. [25], Curto et al. [26], and Merunka et al. [27] analyzed temperature focusing using simple phantoms, primarily adopting circular antenna array configurations or multi-layered cylindrically arranged antennas.

Linear antenna arrays have also been employed in microwave hyperthermia research. Fenn [28] pioneered this approach, utilizing microwave waveguides and breast compression for improved data acquisition and procedural stability. However, Fenn's method involved invasive temperature monitoring using an electric diode, which is impractical for human breasts. Subsequent studies by Dooley et al. [29] and Nguyen et al. [30] expanded upon Fenn's work, incorporating clinical studies and realistic breast models to analyze both heating potential and temperature changes. Nguyen et al. [31] extended their research to different tumor sizes and locations, although not varying breast sizes and densities. Furthermore, experimental studies such as those by Nguyen and Abbosh [32] applied Particle Swarm Optimization (PSO) algorithms.

Various techniques exist for obtaining proper antenna excitations. The time reversal (TR) technique has been widely used in previous hyperthermia studies due to its general applicability [33]–[38]. However, TR's limitation in regulating side lobes often leads to hot spots, particularly in lossy media. Another approach involves optimizing field distribution in the target region using convex programming (CP) strategies [20,21,39,40]. While successful in reducing hot spots, these methods are limited by the problem's nonlinear nature, requiring the objective function to be separated into sub-functions and optimization conducted in parallel. Particle Swarm Optimization (PSO) has been widely used due to its fast convergence; however, it suffers from dependence on initial values, necessitating multiple runs to achieve optimal results. Other proposed approaches, such as the Nelder–Mead simplex algorithm [26], lack PSO's fast convergence but are less sensitive to initial values.

MH necessitates precise calibration of antenna excitations to focus microwave energy selectively on the target area while minimizing impact on surrounding tissue. Various calibration methods exist, including optimization techniques and look-up tables, but they often oversimplify the electric field's complex vector nature and are often system-specific [41]. In this study, an antenna excitation optimization scheme applicable to diverse configurations is introduced. Convolutional neural network (CNN) models for optimization, which outperform traditional look-up tables is employed [41]. This deep-learning-based technique offers a standardized protocol for optimizing antenna excitations in MH applicators and facilitates comparisons between different MH applicators [41].

In Gokyar et. al. [42], it is aimed to predict subject-specific local specific absorption rate (SAR) distributions in the human head. Electromagnetic energy deposition at this field strength is nonuniform, and interference patterns from pTx system channels can lead to increased local SAR values. A multichannel 3D convolutional neural network (CNN) architecture to predict SAR maps and peak-spatial SAR (ps-SAR) levels is developed [42]. By utilizing three channels, each fed by a B_1^+ map, a phase-reversed B_1^+ map, and an MR image, the CNN improved prediction accuracies and reduced uncertainties. The study generated new head-neck body models and MRI data with different RF shim settings to support this approach [42]. The proposed CNN method predicted ps-SAR 10g levels with an average overestimation error of 20%, outperforming virtual observation points-based estimation errors. It also decreased prediction uncertainties by over 20% compared to other methods. The results suggest that multichannel 3D CNN networks hold promise for predicting local SAR values rapidly and accurately, making them clinically useful as an alternative to traditional methods [42].

The facilitation of the development of ultrawideband (UWB) microwave diagnostic and therapeutic technologies, including UWB microwave breast cancer detection and hyperthermia treatment, relies on the accurate understanding of the temperature- and frequency-dependent dielectric properties of biological tissues. In this regard, the temperature-dependent dielectric properties of a representative tissue type—animal liver—are characterized from 0.5 to 20 GHz. Given that discrete-frequency linear

temperature coefficients are impractical and unsuitable for applications spanning broad frequency and temperature ranges, a novel and compact data representation technique is proposed. The dielectric properties data are fitted as a function of frequency using a single-pole Cole–Cole model, and the Cole–Cole parameters are fitted as a function of temperature using a second-order polynomial. This approach allows for the rapid estimation of tissue dielectric properties at any temperature and frequency. The UWB dielectric properties of animal liver tissue have been measured and characterized over the microwave frequency range from 0.5 to 20 GHz and the temperature range from room temperature to $\sim$60 $^{\circ}$C. It has been demonstrated that linear temperature coefficients are impractical and inappropriate over wide frequency and temperature ranges. Instead, a new compact data-cataloging technique has been presented, wherein the frequency dependence of dielectric properties is modeled using a single-pole Cole–Cole model, and the temperature dependence of Cole–Cole parameters is modeled by a second-order polynomial. This simple and elegant technique enables the convenient estimation of liver dielectric properties at any frequencies and temperatures in the specified range [43].

2. MICROWAVE BREAST HYPERTHERMIA TREATMENT PLANNING

2.1 Hyperthermia Treatment Planning

The primary objective of this thesis is to improve the planning process for hyperthermia treatment, with a particular focus on breast cancer. The concept of hyperthermia treatment planning (HTP) is delineated by the Hyperthermia Committee of the American Association of Physicists in Medicine, emphasizing the crucial aspects of selecting the most suitable treatment technique and configuring its geometry. This selection process is based on a comprehensive understanding of the performance characteristics of the available treatment machines and the computational modeling of the expected three-dimensional temperature distribution within the patient. [44]

Following a diagnosis of breast cancer, when a physician determines that hyperthermia therapy is a suitable course of action, the subsequent step involves meticulously planning the treatment regimen. This planning phase is integral to ensuring optimal outcomes and involves a systematic approach to designing the application of microwave hyperthermia specifically designed for breast cancer treatment. The procedure for planning breast microwave hyperthermia therapy is described as follows:

1. Developing the numerical model of the breast.
    (a) Segmentation of the tissue in the high resolution breast image.
    (b) Assignment of thermal and dielectric properties to the tissues.
2. Identifying the appropriate MH applicator for the specific type of breast and tumor.
3. Performing field calculations within the breast model to acquire the distribution of the electric field inside the breast resulting from the radiation emitted by the applicator.

(a) Electromagnetic simulation conducted using both the MH applicator and the segmented breast model.

(b) Prediction of the electric field in a stationary system using the UNET model.

4. Targeted increase in temperature.

(a) Determining the distribution of *SAR* within the breast.

(b) Optimizing the excitation parameters of the applicator (both phase and amplitude) to concentrate the heat energy onto the tumor.

(c) Determining the change in the temperature distribution within the breast based on the optimized *SAR* and the duration of the application.

Throughout the remainder of this chapter, the focus will primarily be on Pennes' bio-heat equation. Subsequently, detailed explanations of the steps undertaken in this thesis to enhance HTP are provided.

2.1.1 Pennes' Bio-Heat Equation

Research on hyperthermia is built upon Pennes' bio-heat equation [47], which outlines the relationship between an external heat source and the consequent changes in tissue temperature. This equation describes the dynamics of heat transfer within biological systems in the following manner:

$$C_p \rho \frac{\partial T}{\partial t} = \nabla \cdot (K \nabla T) + A_0 + \rho SAR - B(T - T_b) \tag{2.1}$$

In this context, C_p represents the specific heat capacity, ρ stands for density, K denotes thermal conductivity, T represents temperature, T_b indicates blood temperature, A_0 signifies metabolic heat generation, and B represents the capillary blood perfusion coefficient. It's worth noting that these terms are specific to each type of tissue. Specific absorption rate (*SAR*) refers to the external heat source, which is the energy deposited per kilogram of tissue. Alternatively, the equation can be formulated as follows:

$$C_p \rho \frac{\partial T}{\partial t} = \nabla \cdot (K \nabla T) + Q_m + Q_0 - B(T - T_b) \tag{2.2}$$

In this equation, Q_m represents metabolic heat generation, while Q_0 corresponds to the heating potential (HP) and is directly proportional to the square of the electric field. The relationship is expressed as $\rho SAR = Q_0 = 0.5\sigma|E|^2$ in units of watts per cubic meter (W/m^3), where E denotes the electric field and σ (S/m) represents the electrical conductivity. Iero et al. [40] demonstrated, employing a Green's function approach, that the peaks of SAR or HP and temperature coincide at the same location assuming constant values for thermal conductivity (K) and capillary blood perfusion coefficient (B) in a steady-state scenario.

2.2 Generating the Numerical Breast Model

2.2.1 Breast tissue segmentation

The breast model utilized in this thesis was acquired from the Phantom Repository at the University of Wisconsin (UWC) [19]. Researchers at UWC meticulously examined MRI images of healthy breasts, segmenting tissues into categories such as muscle, skin, fat, glandular tissues, and a transitional region designated for voxels lacking distinct tissue characteristics. Further segmentation subdivided fat and glands into three sub-tissues. Detailed segmentation procedures and guidance for interpretation can be found in [45]. The MRI scans were captured at a resolution of 0.5 mm, deemed adequate for subsequent analysis. Tissue identification numbers are as follows: Immersion medium: -1, Skin: -2, Muscle: -4, Fibroconnective/glandular-1: 1.1, Fibroconnective/glandular-2: 1.2, Fibroconnective/glandular-3: 1.3, Transitional: 2, Fatty-1: 3.1, Fatty-2: 3.2, Fatty-3: 3.3.

2.2.2 Dielectric and thermal properties

In this section, we explore mathematical models to describe the behavior of dielectric materials, namely the Debye and Cole-Cole models. These models serve as valuable tools in understanding the electrical characteristics of materials, offering insights into their frequency-dependent responses [46].

The Debye model, a fundamental approach in dielectric theory, represents the frequency-dependent dielectric function of a material. It expresses key electrical

Table 2.1 : The Debye parameters of the tissues and the corresponding dielectric constant (ε_r) and electrical conductivity (σ)(S/m) calculated at 2.4 GHz.

Tissue	TypeNo	ε_∞	$\Delta\varepsilon$	σ_s (S/m)	τ (ps)	ε_r	σ (S/m)
Skin	-2.0	15.93	23.83	0.83	13.00	38.84	1.46
Fibroglandular-1	1.1	12.99	24.40	0.40	13.00	36.45	1.04
Fibroglandular-2	1.2	13.81	35.55	0.74	13.00	47.99	1.67
Fibroglandular-3	1.3	14.20	40.49	0.82	13.00	53.13	1.89
Transition	2.0	8.52	20.80	0.41	13.00	28.52	0.96
Fatty-1	3.1	2.85	1.10	0.01	13.00	3.91	0.03
Fatty-2	3.2	3.12	1.59	0.05	13.00	4.65	0.09
Fatty-3	3.3	3.99	3.55	0.08	13.00	7.40	0.17
Muscle	-4.0	21.66	33.24	0.89	13.00	53.62	1.76
Tumor	-	14.20	40.49	0.824	13.00	53.13	1.88

properties such as the dielectric constant (ε_r) and loss factor (ε_i) as a sum of many single-pole oscillators. Known for its simplicity and computational convenience, the Debye model provides a straightforward framework for analyzing dielectric behavior [47]

$$\varepsilon(\omega) = \varepsilon_\infty + \frac{\varepsilon_0 - \varepsilon_\infty}{1 + (i\omega\tau)} \tag{2.3}$$

where $\varepsilon(\omega)$ is the complex dielectric constant, ε_0 is the static dielectric constant, ε_∞ is the high-frequency dielectric constant, ω is the angular frequency, τ is the characteristic relaxation time, and $\Delta\varepsilon = \varepsilon_0 - \varepsilon_\infty$. [47]

In contrast, the Cole-Cole model has a much more complicated structure. It provides a more realistic depiction of actual materials since many practical materials have a frequency-dependent dielectric behavior that is quite complex. The Cole-Cole model includes parallel and series oscillators and many relaxation time constants. This shows amazing dielectric response that can be found in many materials [48].

$$\varepsilon(\omega) = \varepsilon_\infty + \sum_{k=1}^{N} \frac{\varepsilon_0 - \varepsilon_\infty}{1 + (i\omega\tau_k)^\alpha} \tag{2.4}$$

where N is the number of relaxation processes, ε_0 is the static dielectric constant for the k^{th} process, τ_k is the relaxation time for the k^{th} process, α is the Cole-Cole parameter.

Furthermore, we introduce the LEY model, a two-pole model that accounts for both dielectric and thermal properties of materials as functions of temperature [43]. The LEY model describes dielectric properties such as electrical conductivity (σ) and

permittivity (ε) with parameters that vary with temperature, providing a comprehensive framework for understanding the temperature-dependent behavior of materials in 2.5.

$$\varepsilon(\omega,\theta) = \varepsilon_\infty(\theta) + \frac{\Delta\varepsilon_1(\theta)}{1+(i\omega\tau_1(\theta))^{1-\alpha_1}} + \frac{\Delta\varepsilon_2(\theta)}{1+(i\omega\tau_2(\theta))^{1-\alpha_2}} + \frac{\sigma_s(\theta)}{i\omega\varepsilon_0} \tag{2.5}$$

where ε_∞ denotes the permittivity at very high frequencies,ε_0 is the permittivity of free space, $\Delta\varepsilon_{1,2}$ are the dispersion amplitudes and $\tau_{1,2}$ denotes the corresponding relaxation times and σ_s the static conductivity. The parameters $\alpha_{1,2}$ are empirical distribution parameters [43].

For the second step, a second-order polynomial to fit the temperature dependency of the Cole-Cole parameters are adopted. The coefficients for the second-order polynomial are shown in Table 2.2 [43].

$$\begin{aligned}
\varepsilon_\infty(\theta) &= A_1\theta^2 + B_1\theta + C_1 \\
\Delta\varepsilon_1(\theta) &= A_2\theta^2 + B_2\theta + C_2 \\
\tau_1(\theta) &= A_3\theta^2 + B_3\theta + C_3 \\
\Delta\varepsilon_2(\theta) &= A_4\theta^2 + B_4\theta + C_4 \\
\tau_2(\theta) &= A_5\theta^2 + B_5\theta + C_5 \\
\sigma_s(\theta) &= A_6\theta^2 + B_6\theta + C_6 \\
\alpha_1 &= \alpha_2 = 0.4
\end{aligned} \tag{2.6}$$

Table 2.2 : Temperature coefficients of the second-order polynomial fit to the temperature-dependent Cole-Cole parameters for fat tissue.

Parameter	n	A_n	B_n	C_n
ε_∞	1	0.0845×10^{-3} (K^{-2})	-0.0221 (K^{-1})	3.789
$\Delta\varepsilon_1$	2	0.2014×10^{-3} (K^{-2})	-0.0356 (K^{-1})	4.679
τ_1	3	1.163 $(fs\cdot K^{-2})$	-0.2815 $(ps\cdot K^{-1})$	19.74 (ps)
$\Delta\varepsilon_2$	4	0 (K^{-2})	-0.0002 (K^{-1})	15.00
τ_2	5	0.0779 $(ns\cdot K^{-2})$	-9.398 $(ns\cdot K^{-1})$	299.5 (ns)
σ_s	6	0.0043 $(mS\cdot K^{-2})$	0.5504 $(mS\cdot K^{-1})$	18.50 (mS)

The temperature-dependent DPs can be linearized for 37 °C as suggested in Onal et. al. [49]. This model is adopted for this study as in 2.7:

$$\begin{aligned} \varepsilon_r(r,T) &= \varepsilon_r(r,310.15^\circ) \times \left(1 - \frac{T-310.15^\circ}{281.15^\circ} \times \frac{2}{100}\right) \text{ and} \\ \sigma(r,T) &= \sigma(r,310.15^\circ) \times \left(1 + \frac{T-310.15^\circ}{281.15^\circ} \times \frac{10}{100}\right) S/m \end{aligned} \tag{2.7}$$

The dielectric properties of the segmented tissues were also available at [19], taken from the study of [47]. The Debye model was used in this thesis to obtain the corresponding dielectric properties of the breast models [47]. The Debye parameters provided in [45] are calculated for 2.4 GHz, and the conductivity and the relative permittivity values are given in Table 2.1.

The thermal properties of the breast tissues are taken from [15,50]. The thermal properties of the tissues are given in Table 2.3.

Table 2.3 : The thermal properties of the tissues: density (ρ) (kg/m^3), specific heat capacity (C_p) ($J/kg/K$), thermal conductivity (k)($W/m/K$) and metabolic heat generation (Qm) (W/m^3) values.

Tissue	ρ (kg/m^3)	C_p ($J/kg/K$)	k ($W/m/K$)	Qm (W/m^3)
Skin	1200	3300	0.45	368
Fibroglandular	1066	3398	0.33	1180
Transition	1000	2810	0.25	819
Fat	932	2220	0.17	458
Muscle	1085	3800	0.51	684
Tumor	1066	3610	0.51	-

2.3 Selecting a Suitable MH Applicator

This thesis investigated the single-frequency operation of microwave hyperthermia, specifically at 2.4 GHz. In this thesis, 8 dipole antennas operating at 2.4 GHz were utilized.

Many applicator designs have been researched for a successful MH application [51]. In this section, we give the most common MH applicator design for a 2D application, circular array. The geometry for the circular array applicator is shown in Fig. 2.1. In a 2D application, in general, a slice of a breast can be simplified as a circle and a circular array applicator geometry has a perfect fit.

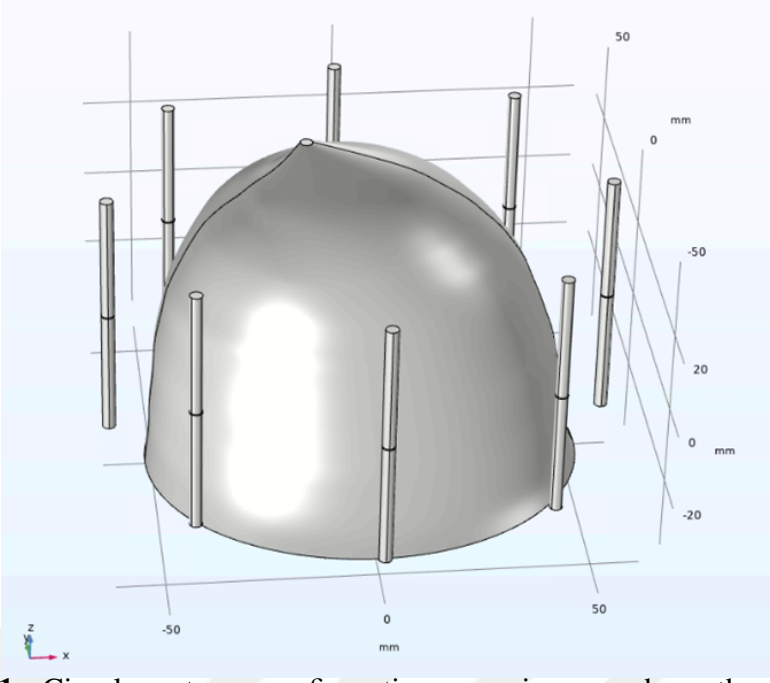

Figure 2.1 : Circular antenna configuration as a microwave hyperthermia (MH) applicator.

2.4 Field Calculations Within the Breast Model

2.4.1 Electromagnetic computation

EM computations were performed using the COMSOL Multiphysics software developed by COMSOL AB. COMSOL is a versatile solver capable of handling multiple physical phenomena simultaneously. It employs the finite element method (FEM) to solve equations. For our electromagnetic (EM) solutions, we utilized the Electromagnetic Wave Physics module within the RF Module.

The geometry of the half-wave dipole antenna was drawn using the geometry module. A uniform lumped port was employed to excite the antenna, with a port impedance of 50 Ω. A zero-phase and 1 V excitation, referred to as unitary excitation, was used in this thesis. 8 circularly positioned antennas constituted the microwave hyperthermia (MH) applicator.

The dielectric properties of the realistic breast, as detailed in Section 2.2, were imported from a text file into COMSOL and interpolated through the breast geometry imported from an .stl file available in [19]. The space surrounding the breast and antennas was assigned the material properties of air. A sphere geometry was generated

to enclose the breast and antennas, serving as the solution domain. A scattering boundary condition was applied to the sphere, while the conducting parts of the antennas were designated as perfectly electric conductor (PEC).

A Frequency Domain study was selected to calculate the wave equation, operating at a single frequency of 2.4 GHz. To generate various electric field distributions inside the breast resulting from different antenna excitations, field properties were calculated with each antenna individually excited with unitary excitation, and then these calculations were repeated for all antennas. Subsequently, the x-, y-, and z-components of the electric field for each excitation were exported to a text file for future use. The interpolated dielectric properties were also exported to ensure that property distributions aligned with the geometric breast phantom.

2.4.2 Total electric field calculation

The electric field components and dielectric values exported from COMSOL were imported into MATLAB (MathWorks). Utilizing the simple superposition principle, any linear combination of electric field distribution within the breast can be generated. The total electric field vector inside the breast with N antenna excitations can be expressed as [52]:

$$\vec{E}_{tot}(r) = \sum_{i}^{N} a_i \vec{E}_i(r) e^{j\phi_i} \; V/m, r \in \Omega \tag{2.8}$$

In this expression, Ω represents the breast domain, $\vec{E}_i(r)$ denotes the electric field vector within the breast when only the i^{th} antenna is excited with unitary excitation, and $a_i e^{j\phi_i}$ represents the i^{th} excitation coefficient, with ϕ_i indicating the phase difference and a_i denoting the amplitude. It's important to note that the phase value of the first antenna was consistently maintained at 0° as a reference point, as the phase value itself serves as a phase difference from the reference phase value.

The magnitude of the complex electric field vector was computed within MATLAB as:

$$\begin{aligned} |\vec{E}_{tot}(r)| &= \sqrt{|E_x^2(r) + E_y^2(r) + E_z^2(r)|} \; V/m \\ \text{where } E_x^2(r) &= (\mathfrak{Re}(E_x) + j\mathfrak{Im}(E_x))^2 \end{aligned} \tag{2.9}$$

The calculation of the x-component of the electric field, given an excitation with a phase difference of ϕ_1 and an amplitude of a_i, is expressed as:

$$E_x(r) = a_i E_{x0}(r) e^{j\phi_i} \; V/m, r \in \Omega \tag{2.10}$$

Here, $E_{x0}(r)$ represents the x-component of the electric field exported from COMSOL.

2.4.3 Focusing of the deposited energy

In microwave hyperthermia, raising the temperature within the breast is achieved by directing RF power to the target region. The success of hyperthermia treatment hinges on effectively concentrating the deposited energy within the target area while minimizing exposure to healthy tissues. This precise localization of energy deposition, known as the focusing of the deposited energy, is crucial for enhancing treatment efficacy and reducing adverse effects.

Mathematically, SAR can be expressed as follows:

$$SAR(r) = \int_{\Omega} 0.5 \frac{\sigma(r)}{\rho(r)} |\vec{E}_{tot}(r)|^2 dV \quad (W/kg) \tag{2.11}$$

where ρ represents tissue density, σ denotes tissue electrical conductivity distribution within the breast, and the integral is taken over the volume Ω.

To enable comparison across different applicators and breast types while enhancing repeatability, the average SAR for the volume Ω is defined as [53]:

$$avSAR_{\Omega} = \frac{\int_{\Omega} SAR dV}{\text{Volume of } \Omega} \quad (W/kg) \tag{2.12}$$

The primary objective of microwave hyperthermia is to increase SAR intensity at the target while maintaining low SAR levels in healthy tissue. To assess this, target-to-breast SAR ratio (TBR_S) and hotspot-to-target SAR quotient (HTQ_S) metrics are utilized:

$$TBR_S = \frac{avSAR_{target}}{avSAR_{breast}} \tag{2.13}$$

$$HTQ_S = \frac{avSAR_{hotspot}}{avSAR_{target}} \tag{2.14}$$

These metrics provide valuable insights into the distribution and concentration of deposited energy within the breast tissue, guiding the optimization of hyperthermia treatment strategies.

2.5 Selective Temperature Elevation

In MH, enhancing the SAR at the target region while minimizing its impact on surrounding healthy tissues is crucial. Optimization techniques are employed to achieve this objective, focusing on antenna excitation parameters such as phase and amplitude. The optimization problem is formulated with the following objective function:

$$\min_{\phi_{1,2,..,N},\, a_{1,2,..,N}} \frac{HTQ_S \cdot avSAR_{healthy}}{TBR_S} \tag{2.15}$$

Since this objective function is nonlinear, linear optimization methods are not applicable. In this thesis, we employ the particle swarm optimization (PSO) algorithm.

2.5.1 Particle swarm optimization

Particle swarm optimization (PSO) is a stochastic optimization technique that operates by guiding particles, forming a swarm, through the solution space. It has gained significant traction in various fields of research. A key characteristic of PSO is its ability to enable particles to learn from their historical positions and performance, as well as from the best-performing particle in the entire swarm. In this thesis, we employ the inertia weighted-PSO algorithm proposed by Shi and Eberhart [54]. The velocity update function is expressed as follows:

$$\begin{aligned} v_{id} = w \times v_{id} + c_1 \times rand([min,max])1 \times (pbestid - x_{id}) \\ + c_2 \times rand([min,max])2 \times (gbestd - x_{id}) \end{aligned} \tag{2.16}$$

$$x_{id} = x_{id} + v_{id} \tag{2.17}$$

In the context of the PSO algorithm, v_{id} represents the velocity of the i^{th} particle in d dimensions, while x_{id} denotes the position of the i^{th} particle in d dimensions. The coefficients c_1 and c_1 are utilized within the velocity update equation, where $rand([min,max])_1$ and $rand([min,max])_2$ are two random numbers generated from a uniform distribution with a range specified by [*min*,*max*], $pbest_{id}$ refers to the personal best (or particle's best) position of the i^{th} particle in d dimensions, while $gbest_d$ represents the global best position among all particles in d dimensions. Additionally, w denotes the inertia weight, serving as an extension to the original PSO algorithm.

We applied PSO to optimize the antenna excitation parameters, especially the phase and amplitude values. The optimization problem's objective function is outlined in Equation 2.15. Considering an antenna applicator with $N = 8$ antennas, we aimed to optimize 7 phase and 8 amplitude values. Notably, we maintained the phase of the first antenna as zero for reference. Consequently, a total of 15 antenna excitation parameters were subject to optimization. The amplitude values were constrained between 0 V and 1 V, and later scaled to provide the required energy for temperature elevation. Similarly, phase values ranged from $-\pi$ to π. To streamline the problem, phase values were initially confined to $[0, 1]$ range, and subsequently remapped to the original range during cost calculation. As a result, the solution space comprised 15 dimensions, with parameter ranges set to [0,1] for each dimension.

In our study, we chose swarm size as 400, iteration number as 500, c_1 and c_2 as 2.0, and w as 1.0. In each iteration, w was decreased with a damping constant of w_{damp}= 0.99. 400 particle objects were created. The position, the velocity, and the corresponding cost of all particles were updated in each iteration. The initial positions were randomly chosen from the d-dimensional solution space while the update function is given in Eq. 2.16.

3. INVESTIGATING THE EFFECT OF TEMPERATURE-DEPENDENT ELECTRICAL PROPERTIES ON HYPERTHERMIA APPLICATION

Dielectric properties play a crucial role in understanding the interaction of electromagnetic fields with biological tissues. These properties, including electrical permittivity and conductivity, are known to exhibit frequency dependency. However, in certain materials like biological tissues, their behavior can also vary with temperature. This chapter explores the implications of temperature-dependent electrical properties on hyperthermia applications, focusing on how changes in dielectric properties influence the efficacy of hyperthermia treatments.

In a study conducted by Ley et al. [43], the authors investigated the temperature and frequency-dependent dielectric changes in porcine adipose tissue. Using a modeling approach based on the two-pole Cole-Cole parameters, they aimed to characterize the complex interplay between temperature, frequency, and dielectric properties. The results of this study shed light on the dynamic nature of dielectric properties in biological tissues under hyperthermic conditions.

Understanding the impact of temperature-dependent dielectric properties is essential for optimizing hyperthermia treatments. By elucidating how changes in tissue properties affect the absorption and distribution of electromagnetic energy, researchers can tailor hyperthermia protocols to maximize treatment efficacy while minimizing potential side effects.

This chapter will delve into the methodology employed by Ley et al. [43] to model temperature-dependent dielectric properties and discuss the implications of their findings for hyperthermia applications. Additionally, it will explore existing literature on similar studies and highlight the significance of considering temperature effects in hyperthermia treatment planning.

In their study, Ley et al. [43] investigated the temperature and frequency-dependent dielectric changes in porcine adipose tissue. They modeled these changes using

the two-pole Cole-Cole parameters. The Cole-Cole parameters are second-degree polynomially dependent on temperature and can be expressed as follows:

$$\varepsilon^*(\omega,T) = \varepsilon_\infty + \frac{\Delta\varepsilon}{1+(i\omega\tau)^\alpha} \tag{3.1}$$

Here, ε^* represents the complex permittivity, ω denotes the angular frequency, T signifies the temperature, ε_∞ is the permittivity at infinite frequency, $\Delta\varepsilon$ represents the change in permittivity, τ is the relaxation time, and α is the Cole-Cole parameter.

For porcine fat tissue, these parameters are shown in the Table 3.1 below:

Table 3.1 : Parameters for porcine fat tissue.

Parameter	Unit	Value at 37°C	Value at 60°C
ε_∞	-	5.4	5.4
$\Delta\varepsilon$	-	13.5	13.5
τ	μs	132.1	75.6
α	-	0.25	0.21

Based on these changes and the study conducted by Onal et al. [49], the following temperature-dependent model has been used for breast tissues:

$$\varepsilon_r(r,T) = \varepsilon_r(r,37^\circ) \times (1 - \frac{T-37^\circ}{8^\circ} \times \frac{2}{100}) \tag{3.2}$$

$$\sigma(r,T) = \sigma(r,37^\circ) \times (1 + \frac{T-37^\circ}{8^\circ} \times \frac{2}{100}) \tag{3.3}$$

Equation 3.2 describes the variation of relative permittivity ε_r with temperature T. It states that the relative permittivity at a specific radial distance r and temperature T is equal to the relative permittivity at the same radial distance and a reference temperature of $\varepsilon_r(r,37^\circ)$, multiplied by a correction factor. This correction factor decreases linearly with the increase in temperature from 37 °C, reducing the relative permittivity with temperature rise. The correction factor is calculated based on the difference between the current temperature T and the reference temperature 37 °C, divided by 8 °C (the range of temperature variation), and then scaled by $\frac{2}{100}$ to adjust the magnitude of the change. Equation 3.3 represents the change in electrical conductivity $\sigma(r,T)$ with temperature T. Similar to Equation 3.2, it describes how the electrical conductivity at a specific radial distance r and temperature T changes concerning the conductivity at the

same radial distance and reference temperature of 37 °C. The electrical conductivity increases linearly with temperature rise, as indicated by the positive slope of the correction factor. The correction factor is computed using the same temperature difference calculation as Equation 3.2, with the same temperature range and scaling factor.

These equations capture the temperature-dependent variations in the dielectric properties of breast tissues, which are crucial for accurately modeling the electromagnetic behavior of tissues during hyperthermia treatments.

In this model, the variation of dielectric properties with temperature is based on the dielectric map at 37 °C and exhibits linear behavior. In the study aimed at heating the upper-left region of the breast model, the antenna parameters obtained through optimization based on the constant dielectric map at 37 °C were subsequently applied to the temperature-varying dielectric map. Hyperthermia treatments were applied for twenty minutes to both constant and variable dielectric maps, and the differences obtained on the maps of electrical permittivity and conductivity are presented below:

In this study, where a total power of $62W$ was supplied to the antennas, the temperature increase achieved after twenty minutes is provided for both the constant $T1$ and variable $T2$ dielectric maps, along with the difference $\Delta T = T1 - T2$.

This study demonstrates that when we achieve a temperature increase of 50 °C with hyperthermia treatment, ignoring the temperature-dependent changes in dielectric properties can result in temperature distributions differing by up to 8 degrees from the expected values. Furthermore, there is not a significant deviation from the target point, and temperature increases can still be achieved in the desired regions. Upon examining the defined hyperthermia performance metrics, it is observed that $TBR_{T1} = 19.55$, $HTQ_{T1} = 0.29$, $avT_{1,healthy} = 0.08$, and $TBR_{T2} = 19.88$, $HTQ_{T2} = 0.30$, $avT_{2,healthy} = 0.07$. The similarity between the metrics is notable, and it is also observed that there is no significant disadvantage in using the antenna parameters obtained based on the constant dielectric map in the actual system. This study has shown that there is no need to recalculate antenna parameters during temperature changes.

3.1 EM Simulation Setup

In this study, COMSOL Multiphysics was utilized with its RF Module and Heat Transfer Module to conduct three-dimensional simulations. The geometry of the breast model was imported into COMSOL for analysis. Initially, both frequency-dependent and time-dependent studies were performed, but it was observed that synchronous changes did not occur. Therefore, a transient frequency-time study was conducted to ensure synchronization between EM field variations and temperature changes (and hence, changes in dielectric properties), leading to accurate results.

The breast model geometry used in the simulations was carefully imported into COMSOL to ensure accurate representation of the tissue structure. The RF Module allowed for the analysis of electromagnetic fields and their interaction with the breast tissue, while the Heat Transfer Module facilitated the investigation of temperature distribution within the tissue.

Initially, frequency-dependent studies were conducted to analyze the response of the breast tissue to varying electromagnetic frequencies. However, it was observed that these studies did not capture the transient nature of the temperature changes induced by the electromagnetic field. Similarly, time-dependent studies were performed to examine the temporal evolution of the temperature distribution. While these studies provided valuable insights into the dynamic behavior of the system, they did not adequately synchronize the changes in the EM field and temperature.

To address this issue, a transient frequency-time study was employed. This study allowed for the simultaneous analysis of EM field variations and temperature changes over time, ensuring synchronization between the two phenomena. By accurately capturing the interplay between EM field fluctuations and temperature dynamics, this approach provided a comprehensive understanding of the thermal response of the breast tissue to hyperthermia treatment.

Overall, the utilization of COMSOL Multiphysics with its RF and Heat Transfer Modules enabled the comprehensive analysis of the electromagnetic and thermal behavior of breast tissue during hyperthermia treatment. The adoption of a transient

frequency-time study ensured synchronization between EM field variations and temperature changes, leading to accurate and reliable simulation results.

3.2 Antenna Excitation Parameter Optimization

The SAR distribution was focused on the target region by optimizing the antenna feeding parameters as in [51]. First, with the DP for 37 °C , the antenna parameters were optimized with PSO. The antennas were fed with $0.8W, 0.53W, 1.62W, 50.0W, 8.53W, 0.48W, 0.02W, 0W$ power respectively. The highest power level of the antenna was taken as $50.0W$ for simulation purposes. The utilized electric field distribution was obtained from the model with temperature-constant DP. In the first part with neglected TP-DP, the optimized antenna parameters were inputted into the COMSOL simulation to obtain the temperature distribution within the breast after 20 minutes of hyperthermia. The increase in the temperature due to the hyperthermia is denoted as T_1. The initial and the ambient temperatures were taken as 310.15°K in the simulations. The thermal properties of the tissues were taken from [43].

3.3 EM Simulation of Temperature-Dependent Dielectric Properties

In the second part, to simulate the co-dependent temperature & DP & electric field change, a temperature-transient study was run on the COMSOL program. Using the same optimized antenna parameters, a second temperature distribution (the temperature increase is denoted as T_2) within the breast after 20 minutes of hyperthermia was obtained.

As input, we took the DP distribution of our breast model [19] and imported them for geometry inputs. As suggested in Onal et. al. [49], the temperature-dependent DP is adopted for this study and used for transient study denoted as T_2. In the Fig. 3.1 the simulation results are shown.

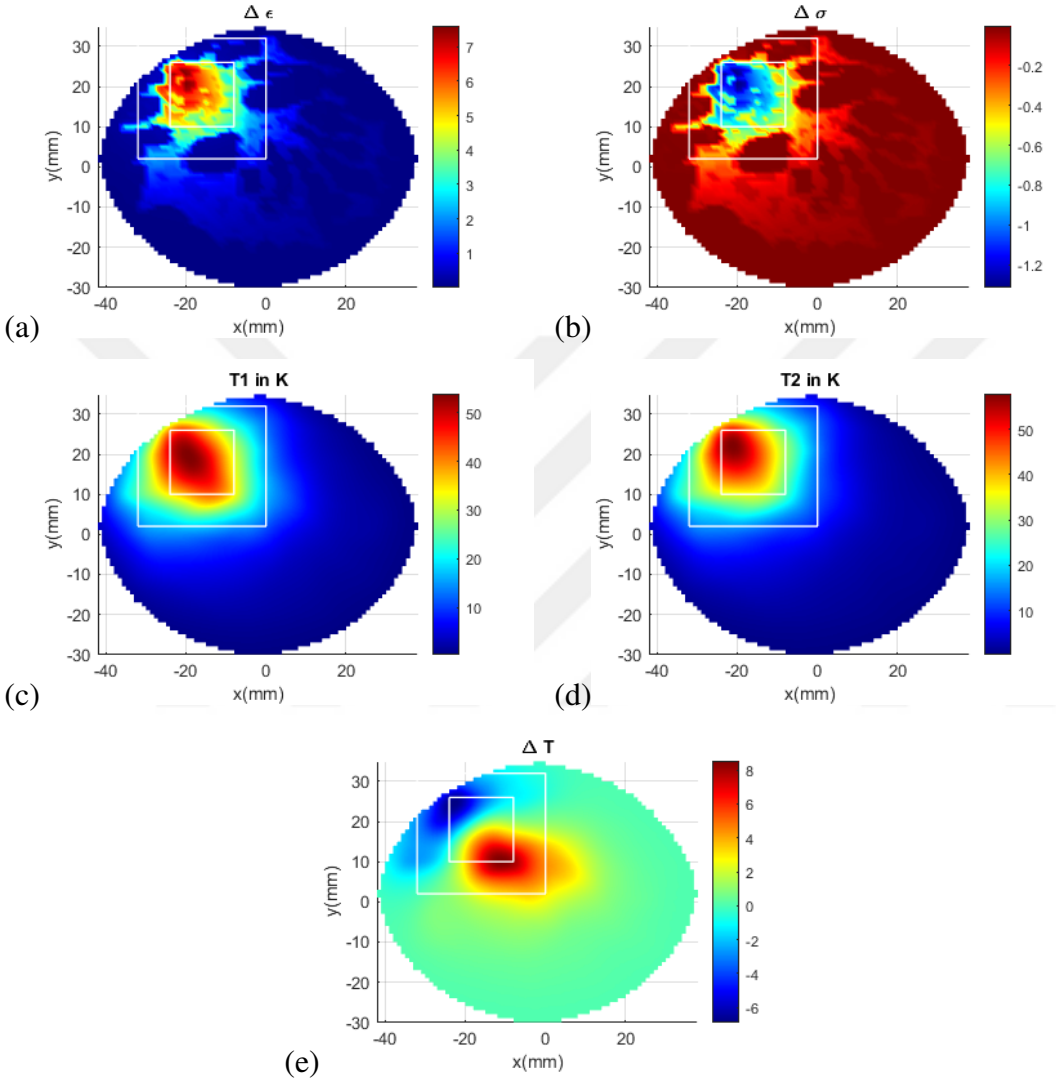

Figure 3.1 : Simulation results after 20 minutes of MH. **(a)** Relative permittivity and **(b)** Electrical conductivity difference due to temperature change. **(c)** Temperature increase in the study with constant breast DP at 310.15 °K. **(d)** Temperature increase in the study with temperature-dependent DP. **(e)** The temperature difference between **(c)** and **(d)** (error due to neglecting TP-DP).

4. ELECTRIC FIELD ESTIMATION FROM DIELECTRIC PROPERTIES TO OVERCOME HEAVY COMPUTATIONAL WORK OF HTP

The process of determining hyperthermia parameters traditionally involves conducting prolonged electromagnetic simulations, which can be computationally intensive and time-consuming. By using artificial intelligence, particularly encoder-decoder architectures, we aim to speed up this process and facilitate the automated generation of hyperthermia parameters. The encoder-decoder architecture, exemplified by the U-Net model, offers a promising approach due to its ability to effectively capture spatial relationships in input data and produce accurate predictions.

This chapter highlights the potential of artificial intelligence, particularly the U-Net model [55], in automating the generation of hyperthermia parameters. By harnessing the capabilities of artificial intelligence, we aim to reduce the computational burden associated with simulation-based approaches and accelerate the optimization of the parameters of hyperthermia treatment. The subsequent sections of this thesis will explain the methodology employed for training and evaluating the U-Net model and present the results obtained from our experiments.

4.1 Why U-Net and What is U-Net?

The U-Net model, characterized by its U-shaped architecture and skipping connections, has gained significance in various image processing tasks, including semantic segmentation and medical image analysis [55]. In the context of hyperthermia, the U-Net model serves as a powerful tool for learning the complex mapping between the geometry of the breast tissue and the resulting electrical field distribution. By training the U-Net model on a diverse dataset comprising different breast models and DP distributions, we aim to develop a robust and generic framework for predicting electrical field distributions.

The choice of U-Net architecture for our research stems from its remarkable performance in semantic segmentation tasks, particularly in the biomedical imaging domain. U-Net has demonstrated superior accuracy and efficiency in segmenting anatomical structures from medical images, making it an ideal candidate for our study objectives. Additionally, the architecture's ability to handle limited training data and its robustness to class imbalance further motivated its selection for our research [42].

To navigate overfitting and enhance generalization, U-Net often incorporates data augmentation techniques during training. Augmentation methods such as rotation, flipping, scaling, and elastic deformations augment the training dataset, thereby diversifying the available samples and improving the model's robustness.

U-Net represents a powerful and versatile architecture for biomedical image segmentation tasks. Its unique design, coupled with its ability to capture contextual information and preserve spatial details, makes it well-suited for our research objectives. By leveraging the capabilities of U-Net, we aim to achieve accurate and reliable segmentation results in our study.

4.1.1 Architecture of U-Net Model

The U-Net model utilizes an encoder-decoder architecture, which is a deep learning architecture. The encoder part consists of a series of convolutional layers that extract feature maps from the input image. The decoder part, on the other hand, involves non-convolutional operations to upsample these feature maps to the dimensions of the input image. This structure can be particularly effective in tasks requiring precise segmentation at the pixel level. Fig 4.1 demonstrates the architecture of the U-Net model [55].

The key feature of U-Net consists of U-Shaped Architecture. U-Net derives its name from its distinctive architecture, which resembles the letter "U." This architecture consists of a contracting path, followed by an expansive path, facilitating the extraction of hierarchical features at different scales [55]. Fig. 4.1 represents the architecture of the U-Net model used.

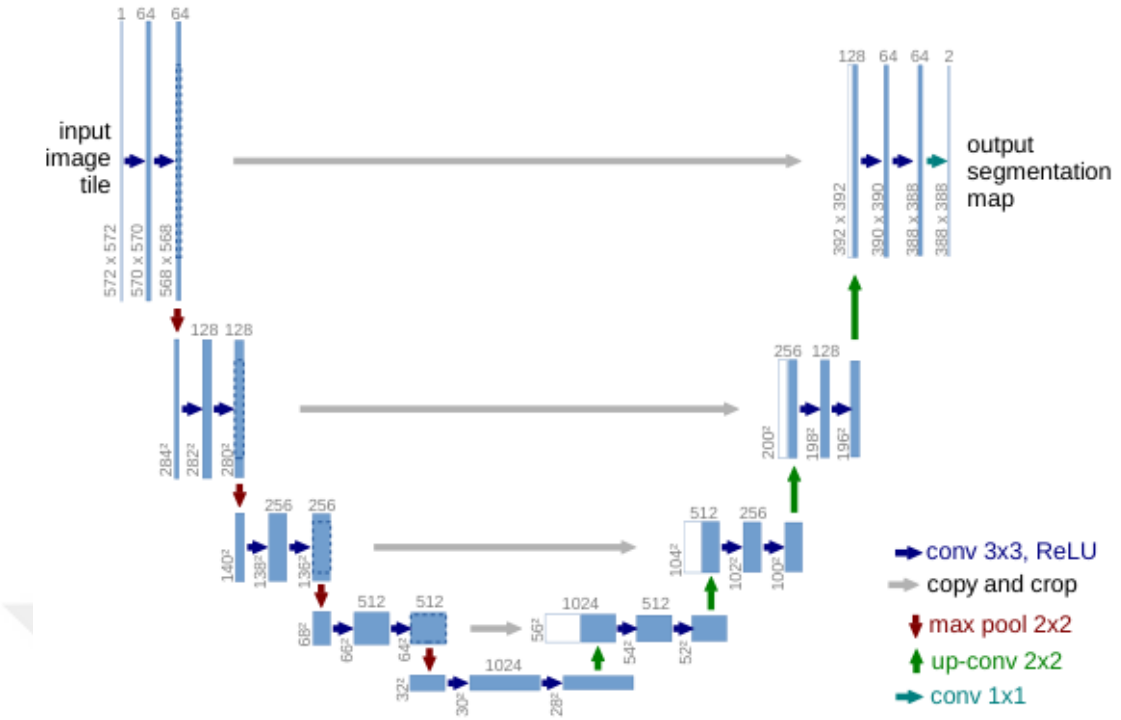

Figure 4.1 : The U-net architecture (illustrated here with a 32x32 pixel example in the lowest resolution) consists of multiple blue boxes, each representing a multi-channel feature map. The number of channels is indicated at the top of each box, while the x-y size is displayed at the bottom left corner. White boxes signify copied feature maps, and arrows indicate the various operations performed within the architecture [55].

One of the defining features of U-Net is the incorporation of skip connections between corresponding layers in the contracting and expansive paths. These skip connections enable the direct flow of low-level features to higher-level layers, facilitating precise localization and alleviating the vanishing-gradient problem [55].

U-Net operates as a fully convolutional network (FCN), leveraging convolutional layers for feature extraction and spatial transformation. The absence of fully connected layers enables U-Net to accommodate input images of varying sizes, making it adaptable to different imaging modalities and resolutions. [55]

4.2 Generating Training Data

4.2.1 Input data preparation: 2-D breast model

EM computations were performed using the COMSOL Multiphysics tool. It employs the finite element method (FEM) to solve equations. For our electromagnetic (EM)

solutions, we utilized the Electromagnetic Wave Physics module within the RF Module. The electric field components and dielectric values exported from COMSOL were imported into MATLAB. Utilizing the simple superposition principle. Generating 2-D breast data is explained in detail in Section 2.4. To assess the results of the U-Net algorithm, initial studies were conducted using a two-dimensional breast model and electromagnetic simulations.

4.2.2 Ground truth data preparation: FEM-based EM computation

Circular sections of breast models with varying dielectric properties were created and placed into a two-dimensional model selected in the COMSOL program. A total of $2 \times 340 = 680$ different dielectric maps were applied as the material properties into the circular section, and simulations were performed with a two-dimensional RF source. The x-component of the electric field generated by a single antenna within the breast phantom was recorded.

To expedite preliminary work, we used a 2D COMSOL simulation. In the literature, there have been studies utilizing deep learning models to model the Green's function [56,57]. These studies employed mathematical methods, necessitating the use of analytical antennas. The goal of our work, however, is to work with antennas designed for medical device applications suitable for clinical use. Electromagnetic simulations are required for these studies.

For our preliminary work, to obtain quick results (both in terms of rapid data generation and fast training of regression models), a two-dimensional simulation environment was established, and data were collected. Unfortunately, a three-dimensional antenna cannot be used in a two-dimensional study; instead, a line source was used. In future work, the actual antenna itself will be utilized.

For each cross-section, dielectric properties obtained from different frequency points were used to augment the data and create a training set. The two-dimensional electrical conductivity and relative permittivity maps of the breast phantom were used as input to the U-Net, and the real part of the two-dimensional electric field was used as output.

4.3 Training and Results

Training of the U-Net model was conducted with the input of two-channel data in the shape of $340 \times 256 \times 256 \times 2$. Input data consists of 340 samples of relative permittivity and electrical conductivity. Our labels in this model consist of the E-Field distributions -normalized between [1,2]- related to the DPs given as input. Label data is in the shape of $340 \times 256 \times 256$. Training process conducted with 100 epochs, batch size 32, and validation split rate as 20%. In this system, Adam optimizer selected and learning rate chosen as 10^{-4}. The loss function has been used as mean squared error, and the segmentation capability has been replaced with regression capability.

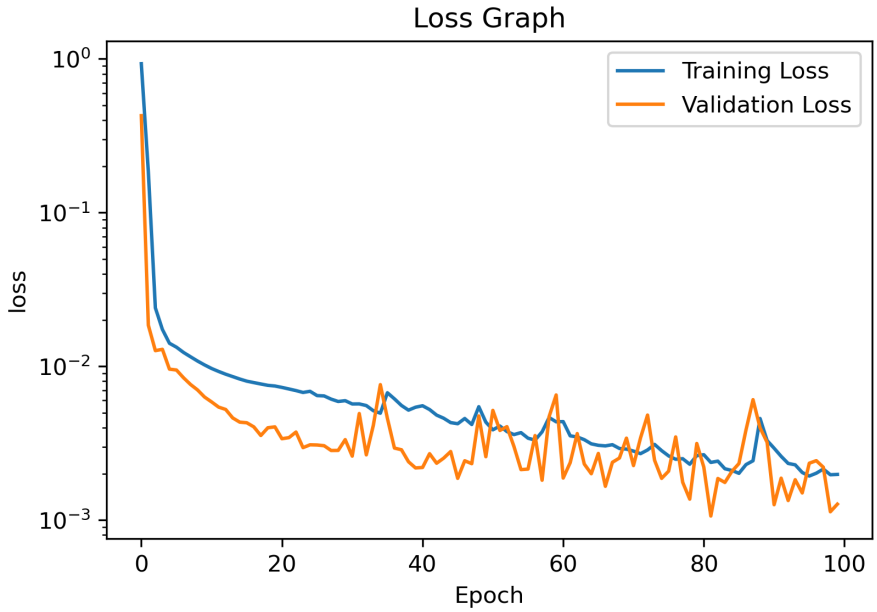

Figure 4.2 : The loss graph of the U-Net model.

After completing the training process, our loss graph is shown in Fig. 4.2. At epoch 100 our loss MSE converges to 0.0016. This can be interpreted as the desired outcome since it is significantly low, close to 0. Therefore we can conclude that the learning process of this model is successful.

The prediction results are shown in Fig. 4.3. Fig. 4.3(a) denotes the predicted E-Field distribution in breast tissue with given DP. Fig. 4.3(b) shows the ground truth of the

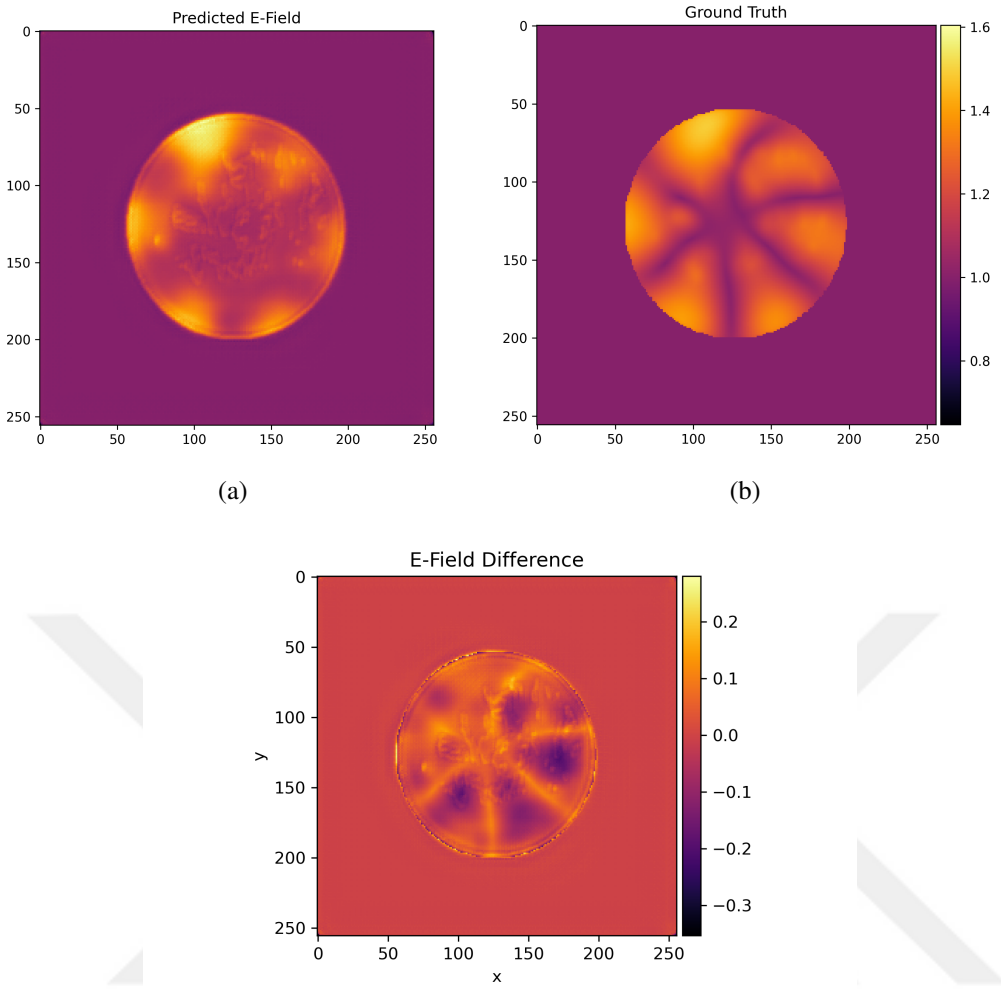

(a) (b)

(c)

Figure 4.3 : Prediction results of U-Net Model. **(a)** Predicted E-Field (V/m) distribution with U-Net model. **(b)** Ground truth of E-Field (V/m) distribution. **(c)** Difference between predicted and ground truth of E-Field distribution (V/m) of breast tissue.

expected result. Fig. 4.3(c) denotes the difference between predicted and expected results. The demonstrated example has a ground truth value between $1-1.6$ in a dataset normalized between $1-2$ and Fig. 4.3(a) and (b) has a common colorbar. The absolute error between the predicted and the ground truth electric fields is less than 0.35.

4.4 Conclusion

Preliminary results indicate promising performance of the U-Net algorithm in predicting the electric field. However, exact field values were not accurately

determined, prompting the need for further training with additional data and training based on electromagnetic theory using Physics-Informed Neural Networks (PINNs). This model will be further developed to accommodate breast phantoms of different sizes and for three-dimensional systems.

The U-Net model shows potential for predicting electric fields, although further refinement and training are required to improve accuracy. The next steps involve training the model with more data and incorporating electromagnetic theory into the training process to enhance its predictive capabilities.

5. HYPERTHERMIA EXPERIMENTAL SYSTEM

5.1 Tissue-Mimicking Phantom Preparation

In this chapter the setup of the microwave hyperthermia treatment system will be given. Furthermore, the calibration procedure of the hyperthermia system as well as the phantom preparation will be provided.

5.1.1 Phantom preparation

Microwave heating is a widely employed method for various applications due to its efficiency and convenience. In this section, we outline the experimental setup and procedures based on the guidelines provided in the study by Lazebnik et al. [47].

Heating Device: The heating device used in our experiments is a standard hot water bath setup. This apparatus serves the purpose of heating liquid samples to desired temperatures. It is equipped with temperature control features and timers for precise adjustments. Pure water should be used inside the water bath to prevent calcification etc.

Precision Measurement: Our experimental setup boasts exceptional precision in measurements to ensure accurate results. For volumetric measurements, we utilize laboratory-grade beakers and measuring cylinders. These instruments offer high precision and reliability in volume measurements. It's worth noting that, during measurements, a measuring cylinder is preferred over a beaker as it provides more accurate volume readings.

Stirring and Thermoregulation: A magnetic stirring bar (or fish) system is employed in conjunction with a magnetic stirrer to facilitate thorough mixing of the liquid samples. Additionally, a built-in temperature sensor within the hot water bath enables real-time monitoring and control of the temperature. It is imperative to maintain

precise temperature control during mixing to prevent any chemical bonding issues and ensure the effectiveness of the heating process.

Preparation of Phantom: Once the experimental setup is ready, the phantom preparation begins. We prepare the phantom using a 16oz thin plastic container compatible with microwave heating (resistant to both temperature and EM wave interactions). The liquid mixture is carefully poured into the containers, ensuring that they are tightly sealed to prevent evaporation during the heating process.

The experimental setup described above adheres to the recommended guidelines for microwave heating experiments outlined by Lazebnik et al. [47]. By meticulously following these procedures, we ensure accurate and reliable results in our microwave heating experiments.

In this study, a material mimicking the tissue in which oils are dispersed within gelatin was characterized by combining five substances—deionized water, sunflower oil, gelatin (Fisher Scientific Grade), surfactant (Fairy Platinum dish detergent), and formaldehyde solution (37% by weight)—in different percentages. While following the phantom characterization protocol presented by Lazebnik et al. [47], chemical contents such as n-toluic acid were avoided. The characterization steps are briefly listed below:

i. 190 ml of deionized water was poured into a beaker, and while stirring the mixture, 34 g of granular gelatin was slowly added.

ii. The mixture was covered with cling film and placed in a hot water bath, heated above 80°C, and maintained until a clear yellow solution was obtained.

iii. The desired amount of melted gelatin was submerged in a cold water bath and placed on a magnetic stirrer at 50°C. While stirring, sunflower oil was slowly added at 120 to 150 rpm.

iv. When the oil was dispersed into the mixture and the mixture turned a lighter yellow, the surfactant was added. Note: If the oil amount exceeds 50%, only 50% of the oil should be added to the melted gelatin first, and after achieving a homogeneous mixture,

the surfactant should be added; the remaining oil should then be slowly added while stirring the mixture.

v. At the end of Step IV, the mixture should be homogeneous, and the color should turn white as the amount of oil increases. When the phantom temperature drops to 35-40°C, the formaldehyde solution is added.

The recipes for the three phantoms used in this study are shown in the table below. The characterized phantoms were poured into 800 ml beakers and covered with cling film to prevent drying. The phantoms were left to harden at room temperature (25°C) for 24 to 48 hours and then placed in a refrigerator for 3 to 4 days to allow for chemical bonding. Subsequently, the phantoms were removed from the beakers, cut into 6 x 6 x 2.5 cm pieces, and wrapped in cling film for dielectric property measurements dependent on temperature [47].

5.1.2 Microwave dielectric spectroscopy

For accurate dielectric measurements, we utilize the state-of-the-art Dielectric Analyzer Kit (DAK). This equipment is specifically designed for conducting precise dielectric measurements across a wide range of frequencies. The DAK apparatus offers high sensitivity and reliability, making it suitable for our experimental requirements.

The experimental setup is meticulously designed to ensure consistency and accuracy in dielectric measurements. The setup includes the integration of the DAK equipment for dielectric characterization. Additionally, the phantom samples are carefully prepared and positioned within the measurement setup to minimize external interference and ensure reliable data acquisition.

The measurement procedure follows a standardized protocol to obtain dielectric data across varying frequencies. Initially, the phantom samples are prepared in accordance with established protocols. Subsequently, the samples are subjected to dielectric measurements using the DAK equipment. The measurements are performed systematically across a predetermined frequency range, with careful attention to calibration and data acquisition procedures.

The dielectric characterization of the phantoms is conducted using the advanced Dielectric Analyzer Kit (DAK) in adherence to the protocols outlined in the study. By following rigorous experimental procedures and utilizing state-of-the-art equipment, we ensure accurate and reliable dielectric measurements essential for comprehensive characterization of the phantom samples.

5.2 Hyperthermia Experimental System Setup

5.2.1 Microwave hyperthermia system components

Microwave hyperthermia systems consist of several crucial components, each playing a vital role in the efficacy and functionality of the overall system. Drawing insights from the study [58] we outline the key subsystem components essential for hyperthermia applications.

RF source: The RF source serves as the primary power provider in the hyperthermia system, supplying the necessary electromagnetic energy to the applicator for heating purposes. It is responsible for generating the desired frequency signals required for tissue heating. In the study, various RF sources may be compared, assessing factors such as output power, frequency stability, and modulation capabilities to optimize hyperthermia treatments.

Amplifiers: Amplifiers play a critical role in boosting the RF signal strength to achieve the desired power levels for effective tissue heating. Different amplifier configurations may be evaluated to determine their efficiency, linearity, and distortion characteristics. In the context of the study, comparisons between amplifier types (e.g., solid-state vs. vacuum tube) may be conducted to ascertain their suitability for hyperthermia applications.

Phase shifters: Phase shifters are utilized to control the phase of the RF signals transmitted by the antenna array. Precise phase control is essential for steering the beam direction and optimizing energy deposition within the target tissue region. The study may explore different phase shifter designs and technologies to assess their performance in achieving uniform heating patterns and maximizing treatment efficacy.

Antenna array: The antenna array forms the core of the hyperthermia applicator, responsible for delivering the RF energy to the target tissue. Various antenna configurations, such as dipole antennas or connected arrays, may be evaluated to determine their radiation characteristics, beamforming capabilities, and heating efficiency. Factors such as antenna size, shape, and orientation may also be examined to optimize energy deposition and minimize side effects on surrounding healthy tissues.

Control and monitoring system: The control and monitoring system encompasses the software and hardware components responsible for system operation, parameter adjustment, and real-time feedback monitoring. It enables clinicians to accurately control treatment parameters such as power levels, frequency settings, and phase adjustments. Additionally, it facilitates continuous monitoring of tissue temperature and feedback mechanisms to ensure safe and effective hyperthermia treatments.

The subsystem components outlined above collectively form the backbone of microwave hyperthermia systems, contributing to their functionality, precision, and efficacy in therapeutic applications. By evaluating and optimizing these components based on the insights provided in the study, advancements can be made in hyperthermia technology to enhance patient outcomes and treatment effectiveness.

5.2.2 Hyperthermia system calibration

In order to finely adjust the behavior of the system feeding into the antennas, the RF source and antennas are removed, and the system is controlled via a Vector Network Analyzer (VNA). The VNA allows precise control and measurement of the characteristics of the system. The following are the specifications of the VNA:

- *Frequency Range:* The VNA operates over a frequency range of 70 KHz to 110 GHz.
- *S-parameter Measurement:* The VNA is capable of measuring S-parameters (scattering parameters) such as S_{11}, S_{21}, S_{12}, and S_{22} providing insight into the behavior of the system.

- *Dynamic Range:* It offers a high dynamic range, enabling accurate measurements even in the presence of low-level signals or noise.
- *Calibration:* The VNA is calibrated to ensure accuracy and repeatability of measurements, allowing for precise adjustments to the system.
- *Software Interface:* It is equipped with user-friendly software for controlling the VNA and analyzing measurement data, facilitating efficient experimentation and analysis. Based on these capabilities, the VNA serves as a versatile tool for fine-tuning and controlling the behavior of the system feeding into the antennas, ensuring optimal performance for microwave hyperthermia applications.

To finely tune the system behavior feeding into the antennas, the RF source and antennas are removed, and the system is controlled via VNA. The VNA provides precise control and measurement of the system's characteristics. The VNA operates over a frequency range of 70 KHz to 110 GHz, allowing detailed analysis of the system response. It is capable of measuring S-parameters such as S_{11}, S_{21}, S_{12}, and S_{22}, providing insight into the system's behavior. Additionally, the VNA offers a high dynamic range, ensuring accurate measurements even in the presence of low-level signals or noise. It is calibrated to ensure measurement accuracy and repeatability, facilitating precise adjustments to the system. Equipped with user-friendly software, the VNA allows for efficient control of the system and analysis of measurement data. With these capabilities, the VNA serves as a versatile tool for fine-tuning and controlling the behavior of the system feeding into the antennas, thereby ensuring optimal performance for microwave hyperthermia applications.

5.3 Hyperthermia Experiment Execution

After the completion of calibration, the Vector Network Analyzer (VNA) is disconnected from the system. Subsequently, the antennas and RF source are connected to the setup, ensuring secure and proper connections. The phase shifter (PS) data obtained during the calibration phase are retrieved and applied to the system. Following this step, the phantom, representing the target tissue, is positioned within

the experimental setup, ensuring precise alignment with the antennas for optimal performance.

To verify the functionality of the antennas and the overall integrity of the setup, a comprehensive functionality check is conducted. This involves testing each component individually and ensuring that they are operating as expected. Once it is confirmed that all components are functioning correctly, the next crucial step is to determine the optimal power level required from the RF source. This calculation is essential to achieve the desired temperature increase within the phantom and ensure the success of the experiment.

After determining the appropriate power level, the RF source is activated to initiate the experiment. Throughout the experiment, stringent measures are taken to minimize exposure to unnecessary RF radiation. To achieve this, the RF source is securely placed outside the experimental environment within a Faraday cage. This setup not only ensures the safety of the experimenters but also facilitates efficient start and stop procedures.

Continuous monitoring and observation are maintained throughout the experiment to track the progress and ensure that all parameters are within the desired range. Any deviations or anomalies detected during the experiment are promptly addressed to maintain the accuracy and reliability of the data collected. Upon completion of the experiment, the RF source is deactivated, and the collected data are meticulously analyzed to extract meaningful insights and draw conclusions regarding the performance and behavior of the microwave hyperthermia system.

5.3.1 Experimental results

The aim of the experiment was to elevate the temperature of the phantom at a specific location (-20, -20, -20) mm, with the center of the phantom designated as the reference point. The breast phantom, with a height of 90 mm and a radius of 45 mm, was divided into two equal parts at the $z = 0$ slice. To simulate fat tissue, an 80% oil-in-gelatin mixture was prepared following the guidelines outlined in [59]. The dielectric properties of the fabricated phantom were assessed using a DAK probe,

yielding ε_r = 3.75 and σ= 0.033 S/m at 2.4 GHz. Two measurement points were selected at the z = -20 mm slice: (-20, -20) mm and (0, -20) mm.

The HT applicator consisted of a circular array of 12 dipole antennas, housed within expanded polyethylene foam. Each antenna was linked to an individual 10W RF power amplifier (HI Microwave Technology HIPA02034040) and the corresponding channels of the phase shifter (HI Microwave Technology HPS-1700T6000M), with a 20 dB loss at each channel [51]. These were driven by a 16 dBm signal at 2.4 GHz generated by the microwave source (Agilent Technologies E8257D). The excitation parameters were fine-tuned to adhere to the maximum power inputs permitted by the RF system for each antenna. Using a Vector Network Analyzer (Keysight M9018A PXIe Chasis), adjustments were made to each signal at the antenna input to rectify any imbalances across the amplifiers [51]. Table 5.1 outlines the optimal magnitude and phase values required for each element in the array.

Table 5.1 : Optimised antenna excitation values for the experiment.

Antenna number	1	2	3	4	5	6	7	8	9	10	11	12
Phase(°)	55	13	10	54	142	-78	-95	27	-80	16	-147	-179
Power(W)	7.8	7.3	7.8	5.7	7.3	6.5	6.6	7.2	6.4	3.6	7.2	6.5

The computational results at $x = -20$ mm slice corresponding to the values in Table 5.1 are given in Fig. 5.1(a). The hyperthermia performance metrics are listed in Table 5.2.

Table 5.2 : Hyperthermia performance results at the target point.

TBR_S	HTQ_S	TBR_T	HTQ_T	P_{tot} (W)
12	0.9	3.4	1.1	33

The maximum available power input for each antenna was limited to 7.8 W due to losses at the phase shifter. During the experiment, the initial temperature of the phantom was 18 °C, with the room temperature maintained at 20 °C. Computational analyses were also conducted for treatment duration. The computed temperature distribution and the thermal image captured by a thermal camera (Guide ZC04C2001351) were compared to validate the thermal effects generated by the HT applicator within a 2D plane (XY-plane).

Following the completion of the experiment, the phantom was removed from the applicator, and the upper portion of the phantom was set aside.

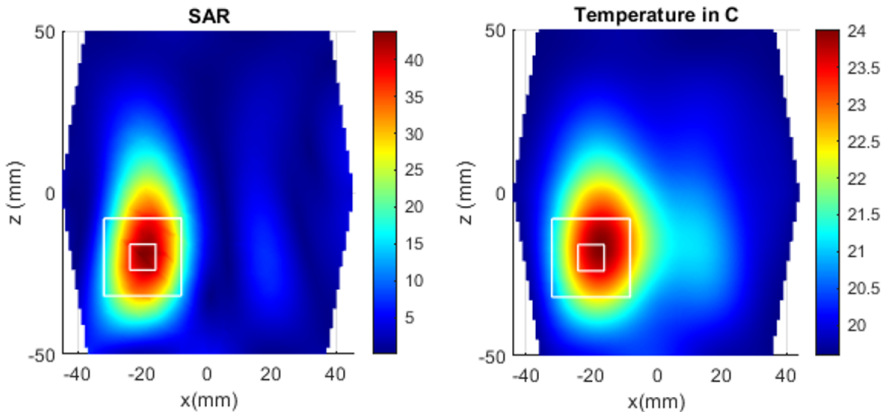

(a)

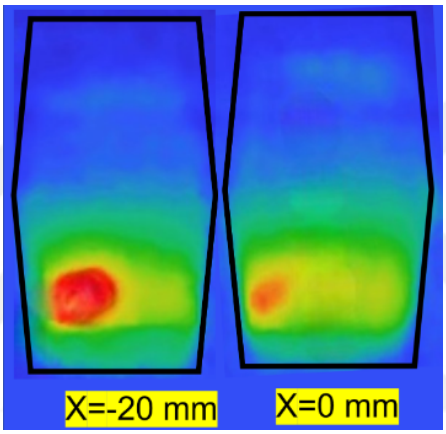

(b)

Figure 5.1 : (a) Computed SAR and temperature distribution at $x = -20$ mm slice. **(b)** Thermal camera image of the MH experiment.

Fig. 5.1(b) shows the thermal camera results for this experiment. Images were taken from x = 0 mm and x = -20 mm slices. The thermal camera utilized during the experiment did not provide specific temperature values or a color bar, thereby hindering the acquisition of precise temperature readings. However, the position of the highest temperature was identifiable and corresponded well with the computed results in Fig. 5.1(a). The experimental outcomes corroborate the computational findings. Discrepancies between the temperature distributions observed in the computed and experimental results may be attributed to the inhomogeneity of the phantom and unknown thermal parameters.

6. CONCLUSIONS

This thesis delved into several key areas related to microwave hyperthermia treatment, analysis of temperature-dependent dielectric properties, and electromagnetic distribution prediction using U-Net architecture. The investigation into microwave hyperthermia treatment revealed the significance of optimizing antenna parameters to achieve desired heating patterns within tissue phantoms. By employing optimization techniques and computational simulations, it was possible to study the effects of antenna configurations on temperature distribution and ensure targeted heating while minimizing damage to surrounding healthy tissues.

Additionally, the analysis of temperature-dependent dielectric properties provided valuable insights into how variations in tissue properties, particularly with respect to temperature, can influence the effectiveness of hyperthermia treatment. By modeling these changes using the Cole-Cole parameters and other established methods, it was possible to develop predictive models that aid in optimizing treatment protocols and improving therapeutic outcomes.

However, it's important to note that high-precision hyperthermia has not yet transitioned into clinical practice due to several reasons. These barriers include technical challenges, computational costs associated with temperature mapping and electromagnetic simulations, and the need for further validation and optimization of treatment protocols. To address these challenges and facilitate the clinical translation of high-precision hyperthermia, ongoing research efforts are underway.

In this thesis, efforts have been made to overcome these barriers by implementing strategies to mitigate computational costs and improve simulation accuracy. Specifically, techniques for optimizing antenna configurations, modeling temperature-dependent dielectric properties, and leveraging machine learning algorithms for electromagnetic distribution prediction have been explored. These

endeavors represent important steps toward realizing the clinical potential of high-precision hyperthermia.

Furthermore, the utilization of U-Net architecture for electromagnetic distribution prediction presented a promising approach for enhancing treatment planning and delivery. Through machine learning algorithms and training on electromagnetic simulations, U-Net demonstrated its potential in accurately predicting the distribution of electric fields within tissue phantoms. This capability holds great promise for optimizing treatment strategies, particularly in scenarios where precise targeting of malignant tissues is paramount.

Looking ahead, future work in this area should focus on continued research and development to further refine and validate the proposed methods. Additional studies are needed to address remaining challenges and optimize hyperthermia treatment protocols for clinical implementation. By addressing these challenges and advancing our understanding of hyperthermia therapy, we can pave the way for its widespread adoption in clinical settings.

The integration of microwave hyperthermia treatment, analysis of temperature-dependent dielectric properties, and electromagnetic distribution prediction using U-Net represent a comprehensive approach to advancing hyperthermia therapy. By leveraging computational simulations, machine learning techniques, and empirical data, this research contributes to the ongoing efforts to improve the efficacy and precision of hyperthermia treatments for various medical applications.

This thesis has explored various aspects related to microwave hyperthermia treatment, including the optimization of antenna parameters regarding temperature-dependent dielectric properties, and the prediction of electromagnetic distribution using U-Net architecture. Through computational simulations and empirical analyses, valuable insights have been gained into the intricacies of hyperthermia therapy, with a focus on enhancing treatment precision and efficacy. Hence, the natural next step was to continue with building the experimental hyperthermia treatment setup. The main building blocks of an experimental system as well as the tissue-mimicking phantom

preparation are explained in detail. The performance of the installed system was verified by a hyperthermia experiment on tissue-mimicking phantom and a high similarity with the computed results was demonstrated.

In conclusion, together all the chapters in this thesis form a detailed roadmap for a breast cancer microwave hyperthermia treatment planning and experimental application.

REFERENCES

[1] **National Cancer Institute** (2021). *Chemotherapy to Treat Cancer*, `https://www.cancer.gov/about-cancer/treatment/types/chemotherapy` [Accessed: Mar. 7, 2024].

[2] **World Health Organization** (2021). *Breast Cancer*, `https://www.who.int/news-room/fact-sheets/detail/breast-cancer` [Accessed: Mar. 7, 2024].

[3] **Paulides, M.**, **Dobsicek Trefna, H.**, **Curto, S. and Rodrigues, D.** (2020). Recent technological advancements in radiofrequency- andmicrowave-mediated hyperthermia for enhancing drug delivery, *Advanced Drug Delivery Reviews*, *163-164*, 3–18.

[4] **Datta, N.**, **Ordóñez, S.**, **Gaipl, U.**, **Paulides, M.**, **Crezee, H.**, **Gellermann, J.**, **Marder, D.**, **Puric, E. and Bodis, S.** (2015). Local hyperthermia combined with radiotherapy and-/or chemotherapy: Recent advances and promises for the future, *Cancer Treatment Reviews*, *41*(9), 742–753.

[5] **Zovathi, B.H.**, **Mohocsi, R.**, **Szosz, A.M. and Cserey, G.** (2022). Breast Tumor Tissue Segmentation with Area-Based Annotation Using Convolutional Neural Network, *Diagnostics*, *12*(9), 2161.

[6] **Strotzer, Q.D.**, **Winther, H.**, **Utpatel, K.**, **Scheiter, A.**, **Fellner, C.**, **Doppler, M.C.**, **Ringe, K.I.**, **Raab, F.**, **Haimerl, M. and Uller, W.e.a.** (2022). Application of A U-Net for Map-like Segmentation and Classification of Discontinuous Fibrosis Distribution in Gd-EOB-DTPA-Enhanced Liver MRI, *Diagnostics*, *12*(8), 1938.

[7] **Chen, W.F.**, **Ou, H.Y.**, **Lin, H.Y.**, **Wei, C.P.**, **Liao, C.C.**, **Cheng, Y.F. and Pan, C.T.** (2022). Development of Novel Residual-Dense-Attention (RDA) U-Net Network Architecture for Hepatocellular Carcinoma Segmentation, *Diagnostics*, *12*(8), 1916.

[8] **Civilibal, S.**, **Cevik, K.K. and Bozkurt, A.** (2022). A deep learning approach for automatic detection, segmentation and classification of breast lesions from thermal images, *Expert Systems with Applications*, *212*, 118774.

[9] **Aydinalp, C.**, **Joof, S. and Yilmaz, T.** (2021). Towards Accurate Microwave Characterization of Tissues: Sensing Depth Analysis of Open-Ended Coaxial Probes with Ex Vivo Rat Breast and Skin Tissues, *Diagnostics*, *11*(2), 338.

[10] **Onemli, E.**, **Joof, S.**, **Aydinalp, C.**, **Pastaci Ozsobaci, N.**, **Ates Alkan, F.**, **Kepil, N.**, **Rekik, I.**, **Akduman, I. and Yilmaz, T.** (2022). Classification of rat mammary carcinoma with large scale in vivo microwave measurements, *Scientific Reports*, *12*(1).

[11] **Istuk, N.**, **Porter, E.**, **OLoughlin, D.**, **McDermott, B.**, **Santorelli, A.**, **Abedi, S.**, **Joachimowicz, N.**, **Roussel, H. and OHalloran, M.** (2021). Dielectric Properties of Ovine Heart at Microwave Frequencies, *Diagnostics*, *11*(3), 531.

[12] **La Gioia, A.**, **Porter, E.**, **Merunka, I.**, **Shahzad, A.**, **Salahuddin, S.**, **Jones, M. and OHalloran, M.** (2018). Open-Ended Coaxial Probe Technique for Dielectric Measurement of Biological Tissues: Challenges and Common Practices, *Diagnostics*, *8*(2), 40.

[13] **Gerazov, B.**, **Caligari Conti, D.A.**, **Farina, L.**, **Farrugia, L.**, **Sammut, C.V.**, **Schembri Wismayer, P. and Conceição, R.C.** (2021). Application of Machine Learning to Predict Dielectric Properties of In Vivo Biological Tissue, *Sensors*, *21*(20), 6935.

[14] **Bonello, J.**, **Demarco, A.**, **Farhat, I.**, **Farrugia, L. and Sammut, C.V.** (2020). Application of artificial neural networks for accurate determination of the complex permittivity of biological tissue, *Sensors*, *20*(16), 4640.

[15] **Said Camilleri, J.**, **Farrugia, L.**, **Curto, S.**, **Rodrigues, D.B.**, **Farina, L.**, **Caruana Dingli, G.**, **Bonello, J.**, **Farhat, I. and Sammut, C.V.** (2022). Review of Thermal and Physiological Properties of Human Breast Tissue, *Sensors*, *22*(10), 3894.

[16] **Burfeindt, M.J.**, **Zastrow, E.**, **Hagness, S.C.**, **Van Veen, B.D. and Medow, J.E.** (2011). Microwave beamforming for non-invasive patient-specific hyperthermia treatment of pediatric brain cancer, *Physics in Medicine & Biology*, *56*(9), 2743.

[17] **Van der Heijden, A.**, **Kiemeney, L.**, **Gofrit, O.**, **Nativ, O.**, **Sidi, A.**, **Leib, Z.**, **Colombo, R.**, **Naspro, R.**, **Pavone, M.**, **Baniel, J.** *et al.* (2004). Preliminary European results of local microwave hyperthermia and chemotherapy treatment in intermediate or high risk superficial transitional cell carcinoma of the bladder, *European urology*, *46*(1), 65–72.

[18] **Giombini, A.**, **Giovannini, V.**, **Cesare, A.D.**, **Pacetti, P.**, **Ichinoseki-Sekine, N.**, **Shiraishi, M.**, **Naito, H. and Maffulli, N.** (2007). Hyperthermia induced by microwave diathermy in the management of muscle and tendon injuries, *British medical bulletin*, *83*(1), 379–396.

[19] (2008). *Phantom Repository*, `https://uwcem.ece.wisc.edu/phantomRepository.html`, [Online; accessed 10-October-2020].

[20] **Iero, D.A.**, **Isernia, T.**, **Morabito, A.F.**, **Catapano, I. and Crocco, L.** (2010). Optimal constrained field focusing for hyperthermia cancer therapy: A feasibility assessment on realistic phantoms, *Progress In Electromagnetics Research*, *102*, 125–141.

[21] **Isernia, T. and Panariallo, G.** (1998). Optimal focusing of scalar fields with arbitrary upper bounds, In Proceedings of the Atti XI Riunione Nazionale di Elettromagnetismo (Italian), (XI RiNEm),.

[22] **Iero, D.A.M.**, **Crocco, L. and Isernia, T.** (2014). Thermal and Microwave Constrained Focusing for Patient-Specific Breast Cancer Hyperthermia: A Robustness Assessment, *IEEE Transactions on Antennas and Propagation*, *62*(2), 814–821.

[23] **Lero, D.**, **Crocco, L. and Isernia, T.** (2017). Advances in 3-D electromagnetic focusing: Optimized time reversal and optimal constrained power focusing, *Radio Science*, *52*(1), 166–175.

[24] **Bellizzi, G.G.**, **Crocco, L.**, **Battaglia, G.M. and Isernia, T.** (2017). Multi-frequency constrained SAR focusing for patient specific hyperthermia treatment, *IEEE Journal of Electromagnetics, RF and Microwaves in Medicine and Biology*, *1*(2), 74–80.

[25] **Elkayal, H.A.**, **Ismail, N.E. and Lotfy, M.** (2015). Microwaves for breast cancer treatments, *Alexandria Engineering Journal*, *54*(4), 1105–1113.

[26] **Curto, S.**, **Garcia-Miquel, A.**, **Suh, M.**, **Vidal, N.**, **Lopez-Villegas, J.M. and Prakash, P.** (2017). Design and characterisation of a phased antenna array for intact breast hyperthermia, *International Journal of Hyperthermia*, *34*(3), 250–260.

[27] **Merunka, I.**, **Fiser, O.**, **Vojackova, L.**, **Vrba, J. and Vrba, D.** (2014). Utilization potential of balanced antipodal Vivaldi antenna for microwave hyperthermia treatment of breast cancer, *The 8th European Conference on Antennas and Propagation (EuCAP 2014)*, IEEE, pp.706–710.

[28] **Fenn, A.J.** (1999). An adaptive microwave phased array for targeted heating of deep tumours in intact breast: animal study results, *International Journal of Hyperthermia*, *15*(1), 45–61.

[29] **Dooley, W.C.**, **Vargas, H.I.**, **Fenn, A.J.**, **Tomaselli, M.B. and Harness, J.K.** (2010). Focused microwave thermotherapy for preoperative treatment of invasive breast cancer: a review of clinical studies, *Annals of surgical oncology*, *17*(4), 1076–1093.

[30] **Nguyen, P.T.**, **Abbosh, A. and Crozier, S.** (2015). Microwave Hyperthermia for Breast Cancer Treatment Using Electromagnetic and Thermal Focusing Tested on Realistic Breast Models and Antenna Arrays, *IEEE Transactions on Antennas and Propagation*, *63*(10), 4426–4434.

[31] **Nguyen, P.T.**, **Abbosh, A.M. and Crozier, S.** (2017). 3-D Focused Microwave Hyperthermia for Breast Cancer Treatment With Experimental Validation, *IEEE Transactions on Antennas and Propagation*, *65*(7), 3489–3500.

[32] **Nguyen, P.T.**, **Abbosh, A. and Crozier, S.** (2017). Three-Dimensional Microwave Hyperthermia for Breast Cancer Treatment in a Realistic Environment Using Particle Swarm Optimization, *IEEE Transactions on Biomedical Engineering*, *64*(6), 1335–1344.

[33] **Fuchs, B. and Fuchs, J.J.** (2011). Optimal Polarization Synthesis of Arbitrary Arrays With Focused Power Pattern, *IEEE Transactions on Antennas and Propagation*, *59*(12), 4512–4519.

[34] **Kosmas, P.**, **Zastrow, E.**, **Hagness, S. and Van Veen, B.** (2007). A Computational Study of Time Reversal Techniques for Ultra-Wideband Microwave Hyperthermia Treatment of Breast Cancer, IEEE, pp.312–316.

[35] **Zastrow, E.**, **Hagness, S.C.**, **Van Veen, B.D. and Medow, J.E.** (2011). Time-Multiplexed Beamforming for Noninvasive Microwave Hyperthermia Treatment, *IEEE Transactions on Biomedical Engineering*, *58*(6), 1574–1584.

[36] **Stang, J.**, **Haynes, M.**, **Carson, P. and Moghaddam, M.** (2012). A Preclinical System Prototype for Focused Microwave Thermal Therapy of the Breast, *IEEE Transactions on Biomedical Engineering*, *59*(9), 2431–2438.

[37] **Trefna, H.**, **Togni, P.**, **Shiee, R. and Persson, M.** (2010). Time-reversal system for microwave hyperthermia., pp.1–3.

[38] **Yavuz, M. and Teixeira, F.** (2005). Frequency Dispersion Compensation in Time Reversal Techniques for UWB Electromagnetic Waves, *IEEE Geoscience and Remote Sensing Letters*, *2*(2), 233–237.

[39] **Iero, D.A.M.**, **Isernia, T. and Crocco, L.** (2013). Focusing time harmonic scalar fields in non-homogenous lossy media: Inverse filter vs. constrained power focusing optimization, *Applied Physics Letters*, *103*(9), 093702.

[40] **Iero, D.A.M.**, **Isernia, T. and Crocco, L.** (2013). Focusing Time-Harmonic Scalar Fields in Complex Scenarios: A Comparison, *IEEE Antennas and Wireless Propagation Letters*, *12*, 1029–1032.

[41] **Yildiz, G.**, **Yasar, H.**, **Uslu, I.E.**, **Demirel, Y.**, **Akinci, M.N.**, **Yilmaz, T. and Akduman, I.** (2022). Antenna Excitation Optimization with Deep Learning for Microwave Breast Cancer Hyperthermia, *Sensors*, *22*(17), `https://www.mdpi.com/1424-8220/22/17/6343`.

[42] **Gokyar, S.**, **Zhao, C.**, **Ma, S. and Wang, D.** (2023). Deep learning-based local SAR prediction using B1 maps and structural MRI of the head for parallel transmission at 7 T, *Magnetic resonance in medicine*, *90*.

[43] **Ley, S.**, **Schilling, S.**, **Fiser, O.**, **Vrba, J.**, **Sachs, J. and Helbig, M.** (2015). Ultra-Wideband Temperature Dependent Dielectric Spectroscopy of Porcine Tissue and Blood in the Microwave Frequency Range, *Sensors*, *15*(7), 16085–16105.

[44] **Dunscombe, P.B.**, **Cetas, T.C.**, **Connor, W.G.**, **Douple, E.B. and Hetzel, F.W.** (1989). *HYPERTHERMIA TREATMENT PLANNING*.

[45] **Zastrow, E.** Database of 3D Grid-Based Numerical Breast Phantoms for use in Computational Electromagnetics Simulations E. Zastrow, SK Davis, M. Lazebnik, F. Kelcz, BD Van Veen, and SC Hagness Department of Electrical and Computer Engineering University of Wisconsin-Madison.

[46] **Lazebnik, M.**, **Popovic, D.**, **McCartney, L.**, **Watkins, C.B.**, **Lindstrom, M.J.**, **Harter, J.**, **Sewall, S.**, **Ogilvie, T.**, **Magliocco, A. and Breslin, T.M.e.a.** (2007). A large-scale study of the ultrawideband microwave dielectric properties of normal, benign and malignant breast tissues obtained from cancer surgeries, *Physics in Medicine and Biology*, *52*(20), 6093–6115.

[47] **Lazebnik, M.**, **Okoniewski, M.**, **Booske, J.H. and Hagness, S.C.** (2007). Highly accurate Debye models for normal and malignant breast tissue dielectric properties at microwave frequencies, *IEEE microwave and wireless components letters*, *17*(12), 822–824.

[48] **Zastrow, E.**, **Davis, S.**, **Lazebnik, M.**, **Kelcz, F.**, **Van Veen, B. and Hagness, S.** (2008). Development of Anatomically Realistic Numerical Breast Phantoms With Accurate Dielectric Properties for Modeling Microwave Interactions With the Human Breast, *IEEE Transactions on Biomedical Engineering*, *55*(12), 2792–2800.

[49] **Onal, H.**, **Yilmaz, T. and Akinci, M.N.** (2023). A BIM-Based Algorithm for Quantitative Monitoring of Temperature Distribution During Breast Hyperthermia Treatments, *IEEE Access*, *11*, 38680–38695.

[50] **Çetingül, M.P. and Herman, C.** (2010). A heat transfer model of skin tissue for the detection of lesions: sensitivity analysis, *Physics in Medicine & Biology*, *55*(19), 5933.

[51] **Yildiz, G.**, **Farhat, I.**, **Farrugia, L.**, **Bonello, J.**, **Zarb-Adami, K.**, **Sammut, C.V.**, **Yilmaz, T. and Akduman, I.** (2023). Comparison of Microwave Hyperthermia Applicator Designs with Fora Dipole and Connected Array, *Sensors*, *23*, 6592.

[52] **Canters, R.**, **Wust, P.**, **Bakker, J. and Van Rhoon, G.** (2009). A literature survey on indicators for characterisation and optimisation of SAR distributions in deep hyperthermia, a plea for standardisation, *International Journal of Hyperthermia*, *25*(7), 593–608.

[53] **Paulides, M.M.**, **Rodrigues, D.B.**, **Bellizzi, G.G.**, **Sumser, K.**, **Curto, S.**, **Neufeld, E.**, **Montanaro, H.**, **Kok, H.P. and Dobsicek Trefna, H.**

(2021). ESHO benchmarks for computational modeling and optimization in hyperthermia therapy, *International Journal of Hyperthermia*, *38*(1), 1425–1442.

[54] **Shi, Y. and Eberhart, R.** (1998). A modified particle swarm optimizer, *1998 IEEE international conference on evolutionary computation proceedings. IEEE world congress on computational intelligence (Cat. No. 98TH8360)*, IEEE, pp.69–73.

[55] **Ronneberger, O.**, **Fischer, P. and Brox, T.** (2015). U-net: Convolutional networks for biomedical image segmentation, *International Conference on Medical image computing and computer-assisted intervention*, Springer, pp.234–241.

[56] **Yao, H.M.**, **Zhang, H.H.**, **Jiang, L. and Ng, M.** (2024). Enhanced Deep Learning Approach for Electromagnetic Forward Modelling of Dielectric Target within the Wide Frequency Band Using Deep Residual Convolutional Neural Network, *IEEE Antennas and Wireless Propagation Letters*.

[57] **Yao, H.M.**, **Jiang, L. and Ng, M.** (2022). Implementing the Fast Full-Wave Electromagnetic Forward Solver Using the Deep Convolutional Encoder-Decoder Architecture, *IEEE Transactions on Antennas and Propagation*, *71*(1), 1152–1157.

[58] **Ahmed, S.K.T.**, **Chowdhury, M.**, **Islam, M.R.**, **Basar, M.G. and Islam, M.S.** (2020). Comparison of Microwave Hyperthermia Applicator Designs with Fora Dipole and Connected Array, *Journal of Electromagnetic Analysis and Applications*, *12*(05), 119–131.

[59] **Lazebnik, M.**, **Madsen, E.L.**, **Frank, G.R. and Hagness, S.C.** (2005). Tissue-mimicking phantom materials for narrowband and ultrawideband microwave applications, *Physics in Medicine & Biology*, *50*(18), 4245.

CURRICULUM VITAE

Name SURNAME: Meltem Duygu ŞAFAK

EDUCATION:

- **B.Sc.:** 2015, İhsan Doğramacı Bilkent University, Engineering Faculty, Electrical & Electronics Engineering Department
- **M.Sc.:** 2024, Istanbul Technical University, Electrical & Electronics Faculty, Telecommunications Engineering Department

PROFESSIONAL EXPERIENCE AND REWARDS:

- 2024 Senior Data Scientist at BiTaksi Mobil Teknoloji A.Ş., Istanbul
- 2022–2023 Senior Data Scientist at NTT Data and Busines Solutions, Istanbul
- 2021–2022 Computer Vision Engineer at Pi Robotik, Istanbul
- 2019–2021 Software Development Engineer at Orion Innovations, Istanbul
- 2016–2019 R&D Engineer at ARÇELİK A.Ş. Central R&D, Istanbul

PUBLICATIONS, PRESENTATIONS AND PATENTS ON THE THESIS:

- **Safak M. D.**, Altintas G. Y. (2024). Impact of Temperature-Dependent Dielectric Characteristics on Microwave Hyperthermia. *3rd International Graduate Research Symposium (IGRS'24)*, May 8-10, 2024 Istanbul, Turkey.
- **Safak M. D.**, Altintas G. Y., Aydinalp C., Akduman I. (2024). Effect of Temperature-Dependent Dielectric Properties of Breast on Microwave Hyperthermia, *2024 IEEE International Symposium on Antennas and Propagation and ITNC-USNC-URSI Radio Science Meeting*, July 14-19, 2024 Florence, Italy